DMD Fast Forward. Published on July 29, 2021 as DOI: 10.1124/dmd.121.000497
This article has not been copyedited and formatted. The final version may differ from this version.

Static and Dynamic Projections of Drug-Drug Interactions Caused by Cytochrome P450 3A Time-Dependent Inhibitors Measured in Human Liver Microsomes and Hepatocytes

Elaine Tseng, Heather Eng, Jian Lin, Matthew A. Cerny, David A. Tess, Theunis C. Goosen, and R. Scott Obach

Medicine Design, Worldwide Research and Development, Pfizer Inc.

Groton, CT

DMD Fast Forward. Published on July 29, 2021 as DOI: 10.1124/dmd.121.000497
This article has not been copyedited and formatted. The final version may differ from this version.

Running Title: Drug Interactions for CYP3A Time-Dependent Inhibitors

Corresponding authors: Elaine Tseng; Pfizer Inc., Eastern Point Road, Groton, CT 06340; elaine.tseng@pfizer.com. R. Scott Obach; Pfizer Inc., Eastern Point Road, Groton, CT 06340; r.scott.obach@pfizer.com.

Number of:

Text Pages: 31

Tables: 7

Figures: 6

References: 78

Words in Abstract: 251

Words in Introduction: 975

Words in Discussion: 2161

Abbreviations: ADME, absorption, distribution, metabolism, and excretion; AUC, area under the concentration vs time curve; AUC_i, area under the concentration vs time curve when co-administered with an inhibitor; AUCR, area under the plasma concentration-time curve ratio in the inhibited and control state; C_{max}, maximum concentration values; C_{avg}, average concentration values; $C_{max,u}$, unbound maximum concentration values; $C_{avg,u}$, unbound average concentration values; P450, cytochrome P450; CYP3A, cytochrome P450 3A4/5; DDI, drug-drug interaction; f_u, fraction unbound; HHEP, human hepatocyte; HLM, human liver microsome; IC_{50}, inhibitory concentration at 50%; [I], inhibitor concentration; $[I]_g$, intestinal inhibitor concentration; $[I]_h$, liver inhibitor concentration; K_i, reversible inhibition constant; K_I, time-dependent inhibition constant; k_{inact}, maximal rate of enzyme inactivation; k_{obs}, rate constant for inhibition; $K_{p,uu}$; unbound partition coefficient in hepatocyte; LC-MS/MS, liquid chromatography-tandem mass spectrometry; m/z, mass to charge ratio; PBPK, physiologically-based pharmacokinetic modeling; TDI, time-dependent inhibition; WEM, William's E medium.

DMD Fast Forward. Published on July 29, 2021 as DOI: 10.1124/dmd.121.000497
This article has not been copyedited and formatted. The final version may differ from this version.

ABSTRACT

Cytochrome P450 3A (CYP3A) is a frequent target for time-dependent inhibition (TDI) that can give rise to drug-drug interactions (DDI). Yet many drugs that exhibit in vitro TDI for CYP3A, do not result in DDI. Twenty-three drugs with published clinical DDI were evaluated for CYP3A TDI in human liver microsomes (HLM) and hepatocytes (HHEP), and these data were utilized in static and dynamic models for projecting DDI caused by inactivation of CYP3A in both liver and intestine. TDI parameters measured in HHEP, particularly k_{inact}, were generally lower than those measured in HLM. In static models, the use of estimated average unbound organ exit concentrations offered the most accurate projections of DDI with geometric mean fold errors of 2.0 and 1.7 for HLM and HHEP, respectively. Use of maximum organ entry concentrations yielded marked overestimates of DDI. When evaluated in a binary fashion (i.e. projection of DDI of 1.25-fold or greater), data from HLM offered the greatest sensitivity (100%) and specificity (67%) and yielded no missed DDI when average unbound organ exit concentrations were used. In dynamic physiologically-based pharmacokinetic modeling, accurate projections of DDI were obtained with geometric mean fold errors of 1.7 and 1.6 for HLM and HHEP, respectively. Sensitivity and specificity were 100% and 67% when using TDI data generated in HLM and Simcyp modeling. Overall, DDI caused by CYP3A-mediated TDI can be reliably projected using dynamic or static models. For static models, average organ unbound exit concentrations must be used as input values otherwise DDI will be markedly overestimated.

DMD Fast Forward. Published on July 29, 2021 as DOI: 10.1124/dmd.121.000497
This article has not been copyedited and formatted. The final version may differ from this version.

SIGNIFICANCE STATEMENT: CYP3A time-dependent inhibitors (TDI) are important in design and development of new drugs. The prevalence of CYP3A TDI is high among newly synthesized drug candidates and understanding the potential need for running clinical drug-drug interaction (DDI) studies is essential during drug development. Ability to reliably predict DDI caused by CYP3A TDI has been difficult to achieve. We report a thorough evaluation of CYP3A TDI and demonstrate that DDI can be predicted when using appropriate models and input parameters generated in human liver microsomes or hepatocytes.

DMD Fast Forward. Published on July 29, 2021 as DOI: 10.1124/dmd.121.000497
This article has not been copyedited and formatted. The final version may differ from this version.

INTRODUCTION

Alterations in the catalytic activities of cytochrome P450 enzymes represent a common mechanism of drug-drug interactions (DDI). Administration of one drug (the "precipitant" or "perpetrator") which inhibits, inactivates, or induces the expression of a P450 enzyme will lead to changes in exposure to a second drug (the "object" or "victim") that is cleared by that enzyme. The scientific and medical literature describe myriad examples of DDI that arise via this mechanism and a large public database that summarizes the knowledge of DDI has been assembled (https://didb.druginteractionsolutions.org/).

Our understanding of the human P450 enzymes and their substrate and inhibitor specificities, along with the development of methods and algorithms to translate in vitro drug metabolism data to in vivo pharmacokinetics through the use of equations and physiologically-based pharmacokinetic (PBPK) modeling platforms, has led to the routine collection of in vitro P450 inhibition data. DDI are an undesired phenomenon in new drugs, and in vitro P450 inhibition data are used in drug design and the selection of candidate compounds for further development as drugs. Such data are also used in developing strategies to evaluate DDI in the clinical phase of drug development, to decide what clinical pharmacokinetic studies need to be conducted in anticipation of observing a DDI (Grimm et al., 2009; Zhang et al., 2010; FDA, 2020).

Among the human P450 enzymes, CYP3A is the most important since it is involved in the metabolic clearance of many drugs (Guengerich, 1995; Zhou, 2008). Thus, this enzyme is of focus for in vitro evaluation of the potential for DDI. Furthermore, this enzyme is prone to time-dependent inhibition (TDI), wherein the degree of inhibition observed increases with increasing incubation time. Some of the most notorious perpetrators of DDI are TDI of CYP3A, including clarithromycin, verapamil, diltiazem, and mibefradil, among others (Backman et al., 1994; Gorski et al., 1998; Mullins et al., 1998; Jones et al., 1999). In fact, mibefradil was withdrawn from clinical use due to CYP3A TDI (Prueksaritanont et al., 1999). Among CYP3A TDI, most are mechanism-based inactivators (MBI) in that the compound must

DMD Fast Forward. Published on July 29, 2021 as DOI: 10.1124/dmd.121.000497
This article has not been copyedited and formatted. The final version may differ from this version.

be acted upon by the enzyme for the inhibition to occur. In P450 incubations, TDI and MBI can be distinguished in that the latter require the inclusion of NADPH, the co-substrate required for P450 catalysis. MBI of P450 enzymes can occur via several biochemical mechanisms and the most well-known are (a) the formation of a complex between a metabolic intermediate of the inactivator and the heme iron (referred to as an M-I complex); (b) adduction of the inactivator to porphyrin, or (c) adduction of the inactivator to the protein backbone of the enzyme. Irrespective of the biochemical mechanism of MBI, all three will result in permanent cessation of the activity of enzyme molecules and DDI, with DDI abating only upon stopping treatment with the perpetrator drug and re-synthesis of the enzyme in vivo (Zhou et al., 2004). Thus, during the drug research and development processes, considerable attention is focused on TDI of CYP3A in order to avoid this unwanted property.

Observations in our laboratories arising through the routine deployment of CYP3A TDI assays (unpublished observations) and those reported by others (Zimmerlin et al., 2011) have shown the preponderance of CYP3A TDI among test compounds to be high. Yet, for several compounds that have shown CYP3A TDI and which were predicted to demonstrate DDI, the result in clinical pharmacokinetic studies with sensitive CYP3A marker substrates, such as midazolam, showed no DDI (Ring et al., 2005; Wang et al., 2013). A reason for this mismatch is currently unknown. Others have attempted to engineer the conditions of in vitro incubations in an attempt to better represent the in vivo situation by the inclusion of plasma in the in vitro incubations (Mao et al., 2011; Mao et al., 2012). In a previous report, it was demonstrated that several drugs that showed measurable TDI of CYP3A in human liver microsomes (HLM) and hepatocytes (HHEP) do not cause DDI in vivo (Eng et al., 2021) . In that work, the focus was on the use of CYP3A TDI data in an early drug research stage when drug design teams are seeking and selecting compounds lacking potential TDI. The conclusion from that study was that a cutoff for the observed inactivation rate constant, k_{obs} (run at a test concentration of 30 μM), is needed under which no compounds will cause in vivo DDI. Even with such a cutoff, several drugs with k_{obs} over that boundary were still not perpetrators of DDI. Such a boundary can be considered over-simplified as it is known that

DMD Fast Forward. Published on July 29, 2021 as DOI: 10.1124/dmd.121.000497
This article has not been copyedited and formatted. The final version may differ from this version.

other factors besides k_{obs} will influence whether a DDI will be observed (e.g. dose and exposure). Nevertheless, this was an important finding and defines a better understanding of how to utilize in vitro CYP3A TDI data in decision-making.

In the present report, the objective was to build upon the observations from Eng and co-workers (Eng et al., 2021) and query the fidelity of CYP3A TDI data in the projection of DDI using measurements of k_{inact} and K_I generated from both HLM and HHEP assays, along with several other necessary input values (e.g. various exposure parameters, plasma free fraction, estimated intestinal exposure, among others). Simple equations that relate in vitro TDI data to in vivo DDI (a.k.a. "static methods") (Ernest et al., 2005; Obach et al., 2007; Grimm et al., 2009) as well as PBPK modeling (a.k.a. "dynamic methods") (Rowland Yeo et al., 2011; Mao et al., 2013) were used and various input parameters are evaluated. These methods were tested with 23 drugs that have reported clinical pharmacokinetic studies with sensitive CYP3A marker substrates (mostly midazolam). This represents the largest dataset for this purpose generated under the same experimental conditions. The results have shown that in vitro TDI data tend to over-project DDI, but that with application of established input parameters success can be obtained using either HLM or HHEP.

DMD Fast Forward. Published on July 29, 2021 as DOI: 10.1124/dmd.121.000497
This article has not been copyedited and formatted. The final version may differ from this version.

MATERIALS AND METHODS

Materials. Research was conducted on human tissue acquired from a vendor that was verified as compliant with internal policies, including IRB/IEC approval. Pooled HLM, consisting of 36 male and 14 female donors, were purchased from Sekisui XenoTech (Kansas City, KS). Cryopreserved pooled HHEP, consisting of 4 male and 6 female donors, pooled mix-gender human plasma collected with K_3EDTA, and male human liver homogenate were purchased from BioIVT (Westbury, NY). Monobasic and dibasic potassium phosphate buffers, magnesium chloride, β-nicotinamide adenine dinucleotide phosphate reduced form (NADPH), HEPES, Dulbecco's phosphate-buffered saline (DPBS), and DMSO were purchased from Sigma (St. Louis, MO). M-PER buffer was purchased from Thermo Fisher Scientific (Waltham, MA). Midazolam was purchased from U.S. Pharmacopeia (Rockville, MD). 1'-Hydroxymidazolam and [$^2H_4$]-1'-hydroxymidazolam were synthesized at Pfizer (Groton, CT). William's E medium was purchased from Gibco (Dublin, Ireland). Commercially obtained chemicals and solvents were of high-performance liquid chromatography or analytical grade. Tested drugs (typical purity >95%) were either synthesized internally at Pfizer (Groton, CT) or purchased from one of the following sources: Sigma-Aldrich (St. Louis, MO), Toronto Research Chemicals (North York, Ontario, Canada), MedChemExpress (Monmouth Junction, NJ), TCI (Portland, OR), or APExBio (Houston, TX).

Identification of Test Drugs. The University of Washington Drug Interaction Database (https://www.druginteractionsolutions.org) was used to compile a list of drugs for which clinical CYP3A inhibition interaction studies were conducted (Table 1). Studies in which midazolam was dosed via the oral route were preferred. In a couple of instances, studies containing midazolam dosed via the intravenous route or other CYP3A probe substrates were chosen. The magnitude of DDI (AUCR) was determined based on the ratio of the probe substrate AUC in the presence (AUC_i) and absence (AUC) of the test drug. For drugs where more than one interaction study

DMD Fast Forward. Published on July 29, 2021 as DOI: 10.1124/dmd.121.000497
This article has not been copyedited and formatted. The final version may differ from this version.

was published at the same dose and route, the weighted average AUCR based on the number of subjects per study was calculated using eq. 1 below:

$$W = \frac{\sum_{i=1}^{n} w_i X_i}{\sum_{i=1}^{n} w_i} \quad \text{(eq. 1)}$$

where the weighted average AUCR (W) is the quotient between the summation of the product of each observed mean AUCR (X_i) and the number of subjects in that study (w_i) divided by the total number of subjects.

Binding to Plasma, Liver Microsomes, and Liver Homogenate. Binding of the test drugs to human plasma, liver microsomes, and liver homogenate were determined based on methods previously described by Di et al. (Di et al., 2017). Briefly, binding experiments were performed by equilibrium dialysis (EqD). The matrix was spiked with 1 µM of test drug (donor) and allowed to dialyze against Dulbecco's phosphate buffered saline DPBS (receiver) for a duration of 6 hours with a 12000-14000 molecular weight cutoff membrane in a humidified incubator supplemented with 5% CO_2 at 37°C. All incubations were performed in quadruplicate. At equilibrium, matrix and buffer samples were collected and matrix matched before addition of 4-volumes of acetonitrile containing a cocktail of internal standards (50 ng/mL tolbutamide and 5 ng/mL terfenadine). Samples were vortexed and centrifuged for 5 minutes at approximately 2300 x *g* at room temperature. The supernatant was collected and analyzed directly by LC-MS/MS (method details are in Supplemental Table 2). Determination of the fraction unbound (f_u) in human plasma, liver microsomes, and liver homogenate were determined by methods described in (Riccardi et al., 2017).

Human Hepatocyte Unbound Partition Coefficient ($K_{p,uu}$). The unbound partition coefficient in HHEP for each of the test drugs was determined following the methods described by Riccardi and co-workers (Riccardi et al., 2018). Briefly, HHEP (0.5 million hepatocytes/mL) suspended in WEM supplemented with L-glutamine and HEPES (50 mM), were incubated with 1 µM of test drug for 2 hours. At the end of the incubation, the HHEP were centrifuged at 40 x *g* for approximately 5 minutes to pellet the cells. The

DMD Fast Forward. Published on July 29, 2021 as DOI: 10.1124/dmd.121.000497
This article has not been copyedited and formatted. The final version may differ from this version.

supernatant was reserved for analysis. The pellet was washed three times with ice cold phosphate buffered saline and the final pellet was lysed with mPER buffer. The reserved supernatant and lysate were matrix matched before the addition of 4-volumes of acetonitrile containing a cocktail of internal standards (200 ng/mL diclofenac and 25 ng/mL indomethacin). Samples were vortexed and centrifuged for 5 minutes at approximately 2300 x *g* at room temperature. The supernatant was mixed with an equal volume of water containing 0.2% formic acid and analyzed directly by LC-MS/MS (Supplemental Table 2). In vitro $K_{p,uu}$ of the test drugs in HHEP were calculated by methods described by Riccardi and co-workers (Riccardi et al., 2018). Partitioning in to hepatocytes was demonstrated to be fairly rapid and equilibrium was generally achieved by 10 minutes (Treyer et al., 2018; Treyer et al., 2019).

IC_{50} determination in Human Liver Microsomes and Human Hepatocytes. HLM and HHEP were used to determine the inhibitory concentration of the test drug to result in 50% (IC_{50}) of CYP3A enzyme activity remaining. HLM incubations (0.01 mg/mL) were supplemented with $MgCl_2$ (3.3 mM) and NADPH (1.3 mM) in potassium phosphate buffer (100 mM, pH 7.4). HHEP (0.2 million hepatocytes/mL) were suspended in WEM supplemented with L-glutamine and HEPES (50 mM). Drug stocks, at incrementing concentrations, were prepared at 100-times the final incubation concentration (up to 100 µM final) in a mixture of organic and aqueous solvents, typically acetonitrile and water (Supplemental Table 1). Midazolam, the probe substrate, was prepared at 10x the final concentration (2-3 µM, corresponding to K_M in HLM and HHEP, respectively) in either potassium phosphate buffer or WEM, for HLM or HHEP, respectively. The final total solvent in the incubations was ≤ 1%. The incubation was initiated with the addition of drug stock immediately followed by the probe substrate. After a 4-minute incubation in HLM or a 10-minute incubation in HHEP, the reaction was terminated by the addition of either two or four volumes of acetonitrile containing internal standard (100 ng/mL [$^2H_4$]1'-hydroxymidazolam) for HLM and HHEP incubations, respectively. All reactions were carried out at 37°C, at a final volume of 200 µL, in duplicate. Samples were vortexed and centrifuged for 5 minutes at approximately 2300 x *g* at room temperature. The supernatant was mixed with an equal

DMD Fast Forward. Published on July 29, 2021 as DOI: 10.1124/dmd.121.000497
This article has not been copyedited and formatted. The final version may differ from this version.

volume of water containing 0.2% formic acid and analyzed directly by LC-MS/MS (methods described below). A standard curve (0.250-250 nM) and inhibitor quality control (iQC, 50 nM) of 1'-hydroxymidazolam was prepared in duplicate at the final protein concentration in the assay for either HLM or HHEP. The inhibitor concentration included in the iQC was determined based on the highest concentration tested in the assay. Standards and iQC samples were processed in the same manner as the incubation samples.

Time-dependent Inhibition in Human Liver Microsomes. Time-dependent inhibition of CYP3A was measured in HLM (0.3 mg/mL) supplemented with $MgCl_2$ (3.3 mM) and NADPH (1.3 mM) in potassium phosphate buffer (100 mM, pH 7.4). Drug stock solutions, at incrementing concentrations up to 300 µM (final), was prepared at 100-times the final incubation concentration in a mixture of organic and aqueous solvents, usually acetonitrile and water (Supplemental Table 1). The final total solvent in the primary incubations was ≤ 1%. The incubation was initiated with the addition of drug stock to the microsomal mixture. At various time points, generally up to 40 minutes, an aliquot of the mixture was transferred to an activity incubation mixture containing midazolam (20.9 µM, 10-fold K_M), $MgCl_2$ (3.3 mM), and NADPH (1.3 mM) in potassium phosphate buffer (100 mM, pH 7.4), generally resulting in a 20-fold dilution. After 6 minutes, the activity reaction was terminated by the addition of two volumes of acetonitrile containing internal standard (100 ng/mL [$^2H_4$]1'-hydroxymidazolam). All reactions were carried out at 37°C, at a final volume of 200 µL, in duplicate. Samples were vortexed and centrifuged for 5 minutes at approximately 2300 x *g* at room temperature. The supernatant was mixed with an equal volume of water containing 0.2% formic acid and analyzed directly by LC-MS/MS (methods described below). A standard curve (0.250-250 nM) and inhibitor quality control (iQC, 50 nM) of 1'-hydroxymidazolam was prepared in duplicate at the final protein concentration in the activity assay. The inhibitor concentration included in the iQC was determined based on the highest concentration tested in the assay divided by the fold-dilution of the primary to secondary incubation. Standards and iQC samples were processed in the same manner as the incubation samples. For several drugs, assay conditions were

DMD Fast Forward. Published on July 29, 2021 as DOI: 10.1124/dmd.121.000497
This article has not been copyedited and formatted. The final version may differ from this version.

modified due to rapid inactivation or potent inhibition of the initial time point. Modifications to the incubation conditions can be found in Supplemental Table 1.

Time-dependent Inhibition in Suspension Human Hepatocytes. Time-dependent inhibition of CYP3A was measured in HHEP in a manner similar to that described by Chen and co-workers (Chen et al., 2011). Drug stock solutions, at concentrations up to 300 µM (final), were prepared at 10-times the final incubation concentration in a mixture of organic and aqueous solvents, usually acetonitrile and water (Supplemental Table 1). The incubation was initiated with the addition of drug stock to HHEP (0.45 million hepatocytes/mL) suspended in WEM supplemented with L-glutamine and HEPES (50 mM), in a total volume of 50 µL. At various time points (typically up to 120 minutes unless otherwise stated) a 200 µL aliquot of the activity incubation mixture consisting of midazolam (final concentration 80 µM, approximately 5-fold K_M) in media was added to the incubation wells, resulting in a 5-fold dilution of the primary incubation. Following a 20-minute activity reaction, the incubation was terminated by the addition of two volumes of acetonitrile containing internal standard (100 ng/mL [$^2H_4$]-1'-hydroxymidazolam). All reactions were carried out at 37°C in a humidified incubator (75% relative humidity, 5% CO_2) in duplicate. The final total solvent in the primary incubations was ≤ 1%. Samples were vortexed and centrifuged for 5 minutes at approximately 2300 x *g* at room temperature. The supernatant was mixed with an equal volume of water containing 0.2% formic acid and analyzed directly by LC-MS/MS (methods described below). A standard curve (0.58-1000 nM) and inhibitor quality control (iQC, 100 nM) of 1'-hydroxymidazolam was prepared in duplicate at the final protein concentration in the activity assay. The inhibitor concentration included in the iQC was determined based on the highest concentration tested in the assay divided by the fold-dilution of the primary to secondary incubation. Standards and iQC samples were processed in the same manner as the incubation samples. For several drugs, assay conditions were modified due to rapid inactivation or solubility limitations of the test drug. Modifications to the incubation conditions can be found in Supplemental Table 1.

DMD Fast Forward. Published on July 29, 2021 as DOI: 10.1124/dmd.121.000497
This article has not been copyedited and formatted. The final version may differ from this version.

LC-MS/MS Methodology for the Quantitation of 1'-Hydroxymidazolam. LC-MS/MS analysis was conducted on either a Sciex 5500 or 6500 triple quadrupole mass spectrometer (Framingham, MA) fitted with an electrospray ion source operated in positive ion mode using multiple reaction monitoring. An Agilent 1290 binary pump (Santa Clara, CA) with a CTC Leap autosampler (Leap Technology, Carrboro, NC) was programmed to inject 10 µL of sample on a Halo 2.7 µm C18 2.1x30 mm column (Advanced Materials Technology, Wilmington, DE). A binary gradient was employed using 0.1% (v/v) formic acid in water (mobile phase A) and 0.1% (v/v) formic acid in acetonitrile (mobile phase B) at a flow rate of 0.5 mL/min. Mass-to-charge (*m/z*) transitions for analytes 1'-hydroxymidazolam and [$^2H_4$]1'-hydroxymidazolam were 342.2 → 324.2 and 346.2 → 328.2, respectively. Analytes were quantified against a standard curve using Analyst software (Sciex). A linear regression with either a weighting of 1/x or $1/x^2$ was used. Standards and iQCs were accepted if the calculated concentrations were ± 25% of their nominal concentration. Acceptance of the iQC demonstrates that the inhibitor did not interfere with 1'-hydroxymidazolam signal on the MS.

Data Analysis

Estimation of K_i. Percent activity remaining of the CYP3A enzyme was determined by normalizing the concentration of 1'-hydroxymidazolam in the presence of varying concentrations of test drug to the concentration of 1'-hydroxymidazolam in the solvent control. The concentration of inhibitor corresponding to a 50% decrease in activity (IC_{50}) was generated using GraphPad Prism 8 (La Jolla, CA). Since inhibition experiments were conducted at the K_M of midazolam, K_i was estimated as IC_{50} divided by two ($IC_{50}/2$) assuming competitive inhibition (Cheng and Prusoff, 1973). Free K_i was determined by correcting K_i with the free fraction determined in microsomes ($f_{u,mic}$) or $K_{p,uu}$ for HLM or HHEP experiments, respectively.

DMD Fast Forward. Published on July 29, 2021 as DOI: 10.1124/dmd.121.000497
This article has not been copyedited and formatted. The final version may differ from this version.

Estimation of K_I and k_{inact}. Data analysis methods previously described by Yates and co-workers (Yates et al., 2012) were used for the estimation of k_{obs}, K_I, and k_{inact}. Briefly, k_{obs} was determined by normalizing the 1'-hydroxymidazolam concentration in each sample to that of the mean solvent control concentration in the initial time point, plotting the natural log of percent remaining activity versus preincubation time, and then calculating the slope of the line ($-k_{obs}$) using the initial linear portion of the curve. A statistical test was done at each concentration of test drug to determine if k_{obs} was statistically different from the within-experiment solvent control, i.e. a parallel lines test, shown in eq. 2.

$$z = \frac{|k_{obs[I]} - k_{obs[0\mu M]}|}{\sqrt{SE^2_{k_{obs[I]}} + SE^2_{k_{obs[0\mu M]}}}} \quad \text{(eq. 2)}$$

Here $k_{obs[I]}$, $k_{obs[0\mu M]}$, and SE represent the inactivation rate for an inhibitor at a single concentration, inactivation rate with solvent control, and standard error, respectively. A statistically significant TDI is defined when the parallel lines test yields a p-value of <0.05. When possible, K_I and k_{inact} parameters were determined using nonlinear regression of the three-parameter Michaelis-Menten equation below:

$$k_{obs} = k_{obs[0\mu M]} + \frac{k_{inact} \times [I]}{K_I + [I]} \quad \text{(eq. 3)}$$

[I] represents the concentrations of the test drug in the primary incubation, k_{inact} is the maximal inactivation rate, and K_I is the inactivator concentration at half k_{inact}.

For compounds where substrate inhibition was observed at the higher concentrations, nonlinear regression of a four-parameter substrate inhibition model (eq. 4) was used to fit the curve.

$$k_{obs} = k_{obs[0\mu M]} + \frac{k_{inact} \times [I]}{K_I + [I] \cdot \left(\frac{1+[I]}{K_i}\right)} \quad \text{(eq. 4)}$$

In the equation above, K_i is a dissociation constant for binding enabling a better fit of the data.

DMD Fast Forward. Published on July 29, 2021 as DOI: 10.1124/dmd.121.000497
This article has not been copyedited and formatted. The final version may differ from this version.

In six instances, the relationship between k_{obs} and [I] did not yield enough of a hyperbola to yield reliable values for K_I and k_{inact}. For these, a composite slope was determined that represents the ratio of k_{inact}/K_I. The static model equations and Simcyp require individual parameters as input values. To accomplish this, $K_{I,u}$ was arbitrarily set at a high value of 1 mM, and the slope was used to calculate k_{inact}. This value for k_{inact} along with the value of 1 mM for $K_{I,u}$ were then used as input values for DDI projections, under the reasonable assumption that $[I]_{in\ vivo} << 1$ mM. For compounds where K_I can be determined, $K_{I,u}$ was determined by correcting K_I with $f_{u,mic}$ or $K_{p,uu}$ for HLM or HHEP experiments, respectively. Analyses were performed using Microsoft Excel (Redmond, WA) and GraphPad Prism 8 (La Jolla, CA).

Predicting Magnitude of DDIs. The magnitude of DDI (AUCR) can be described as a ratio of AUC_i divided by AUC. Mathematical models to determine the extent of DDI while incorporating competitive inhibition and time dependent inactivation in the liver and gut have been extensively described (Rowland and Matin, 1973; Mayhew et al., 2000; Wang et al., 2004; Obach et al., 2006; Obach et al., 2007; Fahmi et al., 2008) and is summarized in the equation below (eq. 5).

$$AUCR = \frac{AUC_i}{AUC} =$$

$$\frac{1}{\left(\left(\frac{1}{1+\frac{[I]_h}{K_i}} \times \frac{1}{1+\left(\frac{k_{inact}\times[I]_h}{(K_I+[I]_h)\times k_{deg,CYP3A,h}}\right)}\right)\times f_{m(CYP3A)}\right)+\left(1-f_{m(CYP3A)}\right)} \times$$

$$\frac{1}{\left(\left(\frac{1}{1+\frac{[I]_g}{K_i}} \times \frac{1}{1+\left(\frac{k_{inact}\times[I]_g}{(K_I+[I]_g)\times k_{deg,CYP3A,g}}\right)}\right)\times\left(1-F_g\right)\right)+F_g} \quad \text{(eq. 5)}$$

In the above equation, k_{deg} represents the hepatic ($CYP_{3A,h}$, 0.00032 min^{-1}) and intestinal ($CYP_{3A,g}$, 0.00050 min^{-1}) degradation rates of the CYP3A enzyme (Obach et al., 2007; Rowland

DMD Fast Forward. Published on July 29, 2021 as DOI: 10.1124/dmd.121.000497
This article has not been copyedited and formatted. The final version may differ from this version.

Yeo et al., 2011). The intestinal k_{deg} is based on a half-life of 23.1 hours, which is the natural turnover rate of enterocytes in vivo (Greenblatt et al., 2003). The hepatic k_{deg} is based on a half-life of 36 hours which was derived from a clinical DDI study conducted by Fromm et al. (Fromm et al., 1996; Obach et al., 2007). The fraction of the victim drug metabolized by the CYP3A enzyme is represented as $f_{m(CYP3A)}$. In this analysis, $f_{m(CYP3A)}$ for the victim drugs midazolam, buspirone, terfenadine, triazolam, and simvastatin are 0.93, 0.94, 0.74, 0.92, and 0.92, respectively (Obach et al., 2006; Yadav et al., 2018). The fraction of the victim drug escaping intestinal metabolism is represented by F_g. For the victim drugs midazolam, buspirone, terfenadine, triazolam, and simvastatin, F_g are 0.57, 0.21, 0.40, 0.75, and 0.66, respectively (Paine et al., 1996; Brown et al., 2005; Galetin et al., 2006; Galetin et al., 2008; Gertz et al., 2008; Shou et al., 2008; Galetin et al., 2010). The terms $[I]_h$ and $[I]_g$ represent inhibiting concentrations of the test drug exposed to the liver and intestine, respectively. Unbound test drug concentrations (C_u) resulting in enzyme inhibition in the liver were estimated as unbound steady state maximum hepatic inlet concentration ($C_{max,hepatic\ inlet,u}$) using the equation below (eq. 6) (Kanamitsu et al., 2000) or unbound steady state maximum ($C_{max,systemic,u}$) or average ($C_{avg,systemic,u}$) systemic concentrations.

$$C_{max,hepatic\ inlet,u} = f_{u,p} \times \left(C_{max} + \frac{F_a \times F_g \times k_a \times Dose}{BPR \times Q_h}\right) \text{ (eq. 6)}$$

In the equation above, k_a is the oral absorption rate of the test drug (or 0.1 min^{-1}), F_a is the fraction of test drug absorbed following oral administration (assume 1), F_g is the fraction of test drug escaping intestinal metabolism (assume 1), $f_{u,p}$ is the free fraction of the test drug in plasma, BPR is the blood-to-plasma ratio (assume 1), and Q_h is the liver blood flow (1617 mL/min (Yang et al., 2007a)).

Test drug concentrations resulting in enzyme inhibition in the intestine were estimated as total or free inhibiting concentrations in the enterocyte (I_g) as defined in eq. 7a by (Rostami-Hodjegan and Tucker,

DMD Fast Forward. Published on July 29, 2021 as DOI: 10.1124/dmd.121.000497
This article has not been copyedited and formatted. The final version may differ from this version.

2004), unbound steady state maximum portal vein concentration ($C_{max,portal,u}$, eq. 7b) or average portal vein concentration ($C_{avg,portal,u}$, eq. 7c).

$$[I]_g = \frac{F_a \times k_a \times Dose}{Q_{ent}} \quad \text{(eq. 7a)}$$

$$C_{max,portal,u} = f_{u,p} \times \left(C_{max} + \frac{F_a \times F_g \times k_a \times Dose}{BPR \times Q_{pv}} \right) \quad \text{(eq. 7b)}$$

$$C_{avg,portal,u} = f_{u,p} \times \left(C_{avg} + \frac{F_a \times F_g \times Dose}{\tau \times BPR \times Q_{pv}} \right) \quad \text{(eq. 7c)}$$

The parameters are the same as described above, with Q_{ent} representing the intestinal blood flow (300 mL/min (Yang et al., 2007b)), Q_{pv} represents the portal vein blood flow (1213 mL/min) which is approximated as 75% of hepatic blood flow and τ is the dosing interval for the inhibitor. Free enterocyte inhibiting concentrations are calculated as $[I]_g$ corrected for $f_{u,plasma}$.

Simcyp Modeling. Simcyp version 19 release 1 (19.0; Certara, Princeton, NJ) was used to simulate the time courses of victim and perpetrator concentrations in plasma. Simulations were conducted using a design of 10 trials with 10 subjects using the age range of 20 to 50 years and 1:1 male to female ratio. Simulations were performed in a virtual population library of healthy volunteers supplied by Simcyp (Sim-Healthy Volunteers). The hepatic and intestinal CYP3A k_{deg} were 0.0193 h^{-1} ($t_{1/2}$=36 h) and 0.03 h^{-1} ($t_{1/2}$ =23 h), respectively, consistent with those used in static modeling. The intestinal concentrations were enterocyte exit concentration (portal vein) with $f_{u,gut} = f_{u,plasma}$ while liver concentrations were liver exit concentration. A summary of the trial designs for all simulations are listed in Table 1. In the DDI studies, the fold-increase in AUCR (e.g., AUC_{inf} ratios in the single-dose studies and AUC_{tau} ratios in the multiple-dose studies) was calculated from the ratios of the simulated values in treatment groups relative to control groups. Geometric means of pharmacokinetic parameters generated from Simcyp simulations were compared with the clinically observed geometric mean parameters. For perpetrator drugs

DMD Fast Forward. Published on July 29, 2021 as DOI: 10.1124/dmd.121.000497
This article has not been copyedited and formatted. The final version may differ from this version.

clarithromycin, diltiazem, erythromycin, paroxetine, simvastatin, and verapamil, compound files were qualified by Simcyp. Azithromycin Simcyp file was developed by Certara using Simcyp V14 and published in Simcyp Global Health Repository. To maintain consistency with the use of input parameters generated internally (i.e. $f_{u,p}$, K_I, k_{inact}, etc.), the steady-state volume of distribution (V_{ss}) and oral clearance (CL_{po}) were adjusted to adequately recover the clinically observed AUC and C_{max} at the dose used in the DDI study. In predicting the inhibitory effect of diltiazem administration, we have incorporated the inhibitory effects of its primary metabolite (MA). Sim-Desmethyldiltiazem (MA) was qualified by Simcyp and used without adjusting V_{ss} and CL. Input parameters of 23 perpetrators are summarized in Supplemental Tables 5-27. Briefly, physicochemical properties (pKa, logP) are obtained from in silico software (ACD/pKa; BioByte). Plasma binding ($f_{u,p}$) was obtained from internal experimental data (Supplemental Table 3). The apparent permeability (P_{app}) values used were either default values included as part of the qualified Simcyp files (Simcyp) or calculated from in silico models (Keefer et al., 2013) and extrapolated to effective permeability in human ($P_{eff,man}$). k_a, V_{ss} and CL_{po} were fitted manually to adequately recover the clinically observed results at the doses used in the DDI studies (Supplemental Table 38). These values were internally consistent with those used in static projections (model 4).

For victim drugs, Sim-Midazolam, SV-Triazolam, and SV-Simvastatin Simcyp library compound files were qualified by Simcyp and used without modification. The terfenadine compound file was developed by Simcyp for QT prolongation prediction and was adjusted to reasonably recover the clinical $f_{m(CYP3A)}$ and F_g. The buspirone Simcyp model was developed based on physicochemical properties, plasma binding, distribution, and elimination obtained from literature (Kivisto et al., 1997; Kivisto et al., 1999; Mahmood and Sahajwalla, 1999). The buspirone model could reasonably recover both PK and $f_{m(CYP3A)}$. Using this model, the predicted AUCR after co-administration of itraconazole are in reasonable agreement with the observed values.

DMD Fast Forward. Published on July 29, 2021 as DOI: 10.1124/dmd.121.000497
This article has not been copyedited and formatted. The final version may differ from this version.

Confusion Matrix Analyses. To determine the success of predicting DDI, contingency tables were analyzed separately for HLM and HHEP results. Cutoff values of AUCR were defined prospectively as ≥1.25-fold (bioequivalence) or ≥2-fold. As an example, in the pairing of clinical and predicted AUCR ≥1.25-fold, true positives (TP) were defined as drugs which resulted in an observed clinical AUCR ≥1.25-fold and were predicted to have an AUCR ≥1.25-fold. True negative (TN) drugs were those that resulted in an observed clinical AUCR<1.25 and were predicted to have an AUCR<1.25-fold. False positive (FP) drugs were defined as observed clinical AUCR<1.25-fold but were predicted to have an AUCR ≥1.25-fold, while false negative (FN) drugs were those where an observed clinical AUCR was ≥1.25-fold but the predicted AUCR was <1.25-fold.

Additional assessments of probability to describe model success included sensitivity, specificity, positive predictive value (PPV), negative predictive value (PPV), positive predictive error (PPE), and negative predictive error (NPE). The sensitivity value describes the ability of the model to correctly identify observed positive DDIs (eq. 8) while the specificity value describes the ability of the model to correctly identify observed negative DDIs (eq. 9). The PPV is the portion of studies that were predicted to have an interaction in the clinic and a clinical interaction was observed (eq. 10). Conversely, the NPV represents the portion of studies that were predicted to not have an interaction in the clinic and a clinical interaction was not observed (eq. 11). The PPE describes the portion of studies that were predicted to have an interaction in the clinic, but a clinical interaction was not observed (eq. 12). Lastly, NPE describes the portion of studies that were predicted to not have an interaction in the clinic, but a clinical interaction was observed (eq. 13).

$$Sensitivity = \frac{TP}{TP+FN} \times 100\% \quad \text{(eq. 8)}$$

$$Specificity = \frac{TN}{TN+FP} \times 100\% \quad \text{(eq. 9)}$$

$$PPV = \frac{TP}{TP+FP} \times 100\% \quad \text{(eq. 10)}$$

DMD Fast Forward. Published on July 29, 2021 as DOI: 10.1124/dmd.121.000497
This article has not been copyedited and formatted. The final version may differ from this version.

$$NPV = \frac{TN}{TN+FN} \times 100\% \quad \text{(eq. 11)}$$

$$PPE = (1 - PPV) \times 100\% \quad \text{(eq. 12)}$$

$$NPE = (1 - NPV) \times 100\% \quad \text{(eq. 13)}$$

Accuracy of Predictions. Accuracy of the various prediction models were assessed by the average fold error (AFE) or bias (eq. 14). Precision of the predictions were evaluated using geometric mean absolute fold error (GMFE, eq. 15) and root mean square fold error (RMSFE, eq. 16). The 90% confidence interval about these errors are calculated using equation 17.

$$AFE = 10^{\frac{\sum log\frac{predicted\ DDI}{actual\ DDI}}{N}} \quad \text{(eq. 14)}$$

$$GMFE = 10^{\frac{\sum\left|log\frac{predicted\ DDI}{actual\ DDI}\right|}{N}} \quad \text{(eq. 15)}$$

$$RMSFE = \sqrt{\frac{\left(log\frac{predicted\ DDI}{actual\ DDI}\right)^2}{N}} \quad \text{(eq. 16)}$$

where N is the total number of predictions.

DMD Fast Forward. Published on July 29, 2021 as DOI: 10.1124/dmd.121.000497
This article has not been copyedited and formatted. The final version may differ from this version.

RESULTS

CYP3A TDI in Human Liver Microsomes and Hepatocytes. Among the 24 compounds evaluated (23 drugs and one metabolite), 23 and 20 demonstrated measurable inactivation kinetic parameters in HLM and HHEP, respectively. Values for K_I ranged from 0.36 to 202 μM in HLM and 0.574 to 51.2 μM in HHEP. These were corrected for unbound fraction prior to utilizing them in projection of DDI (see below). Since hepatocytes are intact cells that possess a membrane barrier, availability of the inhibitor to the CYP enzyme to cause inactivation may be limited, which is not present in HLM. By estimating the intracellular free drug concentration, inhibitor availability to the active site can be determined using $k_{p,uu}$. Therefore, application of $k_{p,uu}$ to HHEP K_I was deemed to be a reasonable estimate of HHEP $K_{I,u}$. For k_{inact}, values ranged from 0.00954 to 0.329 min^{-1} in HLM and 0.00446 to 0.0978 min^{-1} in HHEP. Values are listed in Table 2 and 3 and the percent of control activity vs. incubation time and k_{obs} vs. [I] plots for each drug are shown in the Supplemental Figures. On average (i.e. AFE) the $K_{I,u}$, k_{inact} and $k_{inact}/K_{I,u}$ values in HLM were 1.2-, 3.5-, and 3.2-fold greater than in HHEP.

Projection of DDI from CYP3A TDI Data in Liver Microsomes and Hepatocytes: Static Method. The equations described above were used to make projections of DDI, based on AUCR. While the in vitro kinetic parameters are measured experimentally, several input values needed for these projections cannot be measured experimentally and must be estimated (e.g. F_a, k_a, etc.). Furthermore, the correct in vivo concentrations of the inactivator in the liver and intestine are needed and whether the best values to use are represented by maximum or average organ inlet or egress values is unknown. Based on the input parameters mentioned above, over 50 combinations of these values could be evaluated. These methods were narrowed down to three (referred to as Methods 2-4), selected because they represented internally consistent and physiologically meaningful combinations. That is, we did not further pursue random combinations that would make no sense or be illogically contradictory. These were also compared to the

input parameters currently recommended in the U.S. FDA regulatory document on drug-drug interactions (referred to as Method 1; (FDA, 2020)).

When comparing the approaches, the input parameters of CYP3A degradation rates and organ flow rates were kept constant, as these are reasonably well-established and it was not an objective to test the validity of these values. Also, for many of the drugs used in the evaluation, their overall oral absorption is not known and thus a value of unity was used. This could be an overestimate for some of the drugs. The greatest source of variation in prediction methods lies in the selection of the most relevant in vivo concentrations of the perpetrator drug, in both liver and intestine. In these approaches, unbound concentrations were used, and the concentrations entering the organ (liver and intestine) were compared to concentrations exiting the organ. The concentrations entering the liver were considered as the hepatic inlet estimates ($C_{max,hepatic\ inlet,u}$), whereas the concentrations entering the intestine were estimated using the absorption rate constant and oral doses (eq. 7a). The concentrations exiting the liver and intestine were considered as the systemic concentrations ($C_{max,systemic,u}$ or $C_{avg,systemic,u}$) and estimated portal vein concentrations ($C_{max,portal,u}$, eq. 7b or $C_{avg,portal,u}$, eq. 7c), respectively.

A summary of performance characteristics of DDI prediction from TDI data is presented in Table 4. When using TDI data gathered in HLM in making estimates of DDI, the best input values for concentrations for the liver were the average organ exit values (i.e. $C_{avg,u}$) and the best input values for concentrations for the intestine were also the exit values described by the estimates of portal vein concentrations (Models 3 and 4). Model performance was somewhat better when employing estimated $C_{avg,u}$ values than $C_{max,u}$ values. Model 4 had a geometric mean fold error of 2.0, indicating that on average, projections of DDI from in vitro data were within about 2-fold of the actual values, in this case the 2-fold error favored an overprediction of DDI (Figure 2A). Using organ entrance values for perpetrator concentrations (Models 1 and 2) yielded poorer performance and marked over-projections of DDI. The consideration of using the estimated free concentration in the intestine (Models 2-4) is an

DMD Fast Forward. Published on July 29, 2021 as DOI: 10.1124/dmd.121.000497
This article has not been copyedited and formatted. The final version may differ from this version.

important one. Model 1, as recommended in regulatory guidance, uses a very rapid rate of absorption (proximate to the rate of gastric emptying) and essentially states that the concentration of the perpetrator drug in the enterocyte is equal to the concentration of the total dose dissolved in the lumenal fluids. This yields poor performance and consistent over-projection of DDI from TDI data. Consideration of the free concentration in the enterocytes, along with more realistic absorption rates (Models 2-4), yields a considerable improvement in DDI projection over Model 1.

A similar trend among the use of various input values for in vivo perpetrator drug concentrations was observed when using TDI data from HHEP (Table 4.) Again, Models 3 and 4 which use unbound exit concentrations for liver and intestine yielded the most reliable projections of DDI (Figure 2B, Model 4). Furthermore, use of HHEP TDI data offered nominal performance improvements in projections relative to HLM TDI data, with Model 4 yielding a mean fold error of 1.7, as compared to 2.0 for HLM data. Overall, projections of DDI were still higher than those observed in vivo, especially if organ entrance values for perpetrator concentrations were employed (Models 1 and 2).

Evaluation of AUCR projections relative to the extent of observed clinical AUCR revealed no clear relationship with overpredictions above and below the 2-fold criteria (Figure 3). Of particular interest is significant overpredictions with observed AUCR below 2-fold for several drugs (eg tadalafil, midostaurin) irrespective of in vitro data generated in HLM or HHEP. Further mechanistic evaluation may be required to clarify contributing factors. Drugs with underprediction of DDI using data generated in HHEP were diltiazem (Simcyp only), nelfinavir and conivaptan (static and dynamic modeling).

In addition to evaluating these approaches for numerical accuracy of projection of DDI, it is also useful to evaluate them using categorical criteria and cut-off values for what is defined as a DDI and what is not (i.e. a confusion matrix analysis). This analysis was conducted using two criteria for DDI: 1.25-fold, as defined by bioequivalence boundaries, and 2-fold. The latter is offered as a reasonable value for DDI that

DMD Fast Forward. Published on July 29, 2021 as DOI: 10.1124/dmd.121.000497
This article has not been copyedited and formatted. The final version may differ from this version.

may actually be meaningful for clinical outcome. This will always be dependent on the therapeutic window for the affected drug as some drugs are very safe and marked increases in exposure can still be well-tolerated. But others could be dosed at levels such that smaller increases in exposure can yield meaningful side effects. Nevertheless, very few drugs go from safe to toxic with a mere 2-fold increase in exposure, and thus a 2-fold DDI cutoff criteria was a deemed useful one by which to evaluate these DDI projection methods.

TDI experiments performed in HLM offer very high sensitivity, however specificity can be low, depending on the model employed. When using the data in this binary fashion, the ten drugs (Figure 4) that cause a greater than 2-fold DDI are readily identified irrespective of the model used yielding 100% sensitivity (Table 5). However, this comes at a cost of a high rate of false positives especially when using Models 1 and 2 (organ entrance concentrations as input for in vivo [I]) as 13 of 15 drugs that cause DDI below 2-fold are actually identified as causing greater than 2-fold DDI). The PPE, i.e. the portion of DDI studies that are identified as needing to be conducted but actually are negative and would not need to be conducted, is high at 57%. This attribute improves to 33-50% if Models 3 or 4 are employed in that a greater number of the negative drugs are properly identified as such and this does not come at the expense of any false negative drugs: all positive drugs are identified. Overall, the performance of the models using HLM data is similar when using either 1.25- or 2-fold as the defining cutoff for DDI. When using TDI data generated in HHEP, the PPE improves to a minor extent, decreasing to as low as 25%. However, this comes at a cost of 1-3 instances of false negative outcomes. Overall, the combination that yields the lowest PPE while not giving any false negative is the use of TDI data from HLM entered into Model 4 which uses the average organ exit concentrations for in vivo [I]. This observation is independent of the DDI cutoff applied (i.e. 1.25- or 2-fold).

Projection of DDI from CYP3A TDI Data in Liver Microsomes and Hepatocytes: Dynamic PBPK Method. These in vitro data were also used as input values for projecting DDI using Simcyp. In this

DMD Fast Forward. Published on July 29, 2021 as DOI: 10.1124/dmd.121.000497
This article has not been copyedited and formatted. The final version may differ from this version.

case, various input parameters such as in vivo [I] values, absorption extent and rate values, and enzyme degradation rates are embedded in the algorithms. The output DDI projections were evaluated as above for both numerical accuracy of DDI projections (Table 6) as well as categorical assignment of the potential for DDI using 1.25- and 2-fold boundaries (Table 7). Use of Simcyp yielded overall accuracy for projections of DDI from in vitro data with mean fold errors of 1.7 and 1.6 if data were from HLM or HHEP, respectively (Figure 2 Panels C and D). These performance characteristics are slightly better than the best of the static models (Model 4). When evaluated in a confusion matrix, Simcyp modeling performed very well with TDI data from HLM, with no instances of false negatives (i.e. 100% sensitivity) and with high specificity (PPE of only 24% and 23% when using 1.25-fold and 2-fold cutoff values for defining a DDI (Table 7). However, with TDI data obtained from HHEP, the performance of Simcyp suffered slightly with occurrences of false negatives that decreased sensitivity to about 70-85% depending on cutoff criteria (Figure 5).

DMD Fast Forward. Published on July 29, 2021 as DOI: 10.1124/dmd.121.000497
This article has not been copyedited and formatted. The final version may differ from this version.

DISCUSSION

The projection of clinical DDI from in vitro TDI data is challenging. Considerable progress has been made, yet it is still commonplace to project DDI from in vitro data and then conduct a clinical study based on that projection, only to observe no DDI. In drug development such an occurrence (i.e. a false positive from the in vitro data), while demonstrating that it will be acceptable to co-administer the two agents based on the clinical observation, expends effort on a clinical DDI study that really did not need to be conducted. Efforts and resources would be better expended on other clinical studies. Our exploration of different model input values, especially the application of projected organ egress concentrations instead of entry concentrations improves the overall fidelity of predictions of DDI while still avoiding the occurrence of false negative outputs. Use of PBPK modeling (Simcyp) yielded excellent performance with data from HLM, with no false negative outputs. It is false negative outputs (i.e. projection of no DDI from in vitro data but actual DDI in the clinic) which must be avoided as this would result in a deleterious impact on patient safety.

It should be noted that in vitro TDI assays, using HLM or HHEP, are highly sensitive. If one considers the lower limit of statistically detectable k_{obs} values in vitro (0.002 min^{-1} and 0.0015 min^{-1} for HLM and HHEP, respectively; (Eng et al., 2021)) as compared to the estimate for the natural turnover rate for CYP3A in vivo (0.00032 min^{-1}), then any drug demonstrating measurable TDI would be expected to cause at least a 12-fold decline in CYP3A activity at the inhibitor concentration that yielded the lower limit value of k_{obs}. That is, the rate of inactivation would exceed the natural rate of enzyme re-synthesis by 12-fold. It should also be noted that varying values of $k_{deg,h}$ for CYP3A4 have been reported in the literature (Yang et al., 2008) and that the accuracy of projections of DDIs from in vitro data will be dependent on the $k_{deg,h}$ value used. A value of 0.00032 min^{-1} was selected for our static models to be consistent with the value embedded in the Simcyp algorithm.

DMD Fast Forward. Published on July 29, 2021 as DOI: 10.1124/dmd.121.000497
This article has not been copyedited and formatted. The final version may differ from this version.

The present efforts focused on three main objectives: (1) a comparison of in vitro TDI data generated in HLM and HHEP; (2) evaluation of different input values for estimates of in vivo concentrations of the inhibitor in static models for DDI prediction and identification of the best values; and (3) evaluation of the dynamic PBPK model Simcyp for prediction of DDI from TDI data. The in vitro dataset generated for these objectives represents the largest one reported using a fixed source of in vitro reagents and consistent methods run in one laboratory, paired with clinical DDI data gathered from the literature. Previously reported efforts had many fewer examples included (Mayhew et al., 2000; Obach et al., 2007; Mao et al., 2011; Kenny et al., 2012). CYP3A was the enzyme of focus since the greatest number of TDI and DDI are known for this enzyme. Other CYP enzymes such as CYP2D6 or CYP1A2 have few examples of drugs that are TDI with corresponding clinical data for comparison, and as such do not offer a large enough set of drugs from which conclusions could be drawn. It is proposed that the conclusions generated for CYP3A could be applicable to other enzymes. Also compared to other P450s the magnitude of CYP3A-based DDIs can be high for orally administered drugs because of the potential for inhibition of this enzyme not only in the liver but also in the small intestine during the absorption of the drugs following oral administration.

The data demonstrated that DDI are predictable from in vitro TDI data gathered in either in vitro system. Inactivation kinetic values in HLM were generally greater than in HHEP. In both cases, it was important to correct K_I values generated from nominal concentrations of the inhibitor added to the incubations by binding and partition factors. Inhibitor concentrations available to inactivate CYP3A may actually be lower than those added to the assay due to non-specific binding (HLM and HHEP) and unequal concentrations of unbound drug inside and outside the cell (i.e. $K_{p,uu}$ in hepatocyte incubations). Most important is the selection of the most appropriate value for in vivo concentration of the inhibitor drug. Previous recommendations have advocated that the total concentration of drug in the lumen should be used for projection of DDI occurring in the intestine and unbound maximum concentrations estimated for the portal vein during absorption be used for projection of DDI occurring in the liver (Ito et al., 1998;

DMD Fast Forward. Published on July 29, 2021 as DOI: 10.1124/dmd.121.000497
This article has not been copyedited and formatted. The final version may differ from this version.

Rostami-Hodjegan and Tucker, 2004; FDA, 2020). These are represented in Model 1, and lead to such marked over-projection of DDI (mean-fold errors of 4-6, and high false positive rates) that the value of conducting in vitro TDI assays is essentially negated. The assay would be futile as just about every drug tested will suggest the likelihood of DDI and the need for a clinical DDI study. However, moving to potentially more realistic values for in vivo [I] in intestine (enterocytes) and in liver greatly improves the accuracy of DDI projection. In Models 3 and 4, estimated unbound organ exit concentrations are used (i.e. free portal concentrations for intestine and free systemic concentrations for liver) and these may better reflect the concentrations of inhibitor available to affect the enzyme in these tissues. Use of $C_{avg,u}$ values were shown to be best. Mean fold accuracy values of 2.0 and 1.7 were calculated when using HLM and HHEP data, respectively (Table 4). Simcyp modeling, in which the relevant in vivo concentration values are embedded in the software, yielded mean fold accuracy values of 1.7 and 1.6 for HLM and HHEP, respectively (Table 6). Furthermore, a high degree of correlation (r^2>0.9) was observed when predicted AUCRs from HLM and HHEP using Model 4 and Simcyp were compared (Figure 6). These performance characteristics for both static and Simcyp modeling demonstrate that DDI can be projected from in vitro TDI data provided that appropriate input values are entered. Additionally, the use of HHEP generated TDI values with Simcyp modeling would provide an estimated AUCR with the highest degree of numerical accuracy compared to clinical observations.

A second manner in which in vitro TDI data may be used is in a binary decision-making fashion. Thus, instead of seeking numerical accuracy in projecting DDI, the data are used to determine whether a clinical DDI study is needed or not. This depends on the cutoff used to define a DDI and in this analysis the data were evaluated using two cutoff criteria: 2-fold representing a minimum of what may cause a clinically meaningful DDI for many drugs and 1.25-fold representing a conservative bioequivalence boundary. Utilizing the data in this manner strives for minimizing false positives (i.e. running a clinical DDI study which shows no DDI) while not allowing for any false negatives (i.e. not running a clinical DDI study when one was actually needed). As with the aforementioned numerical accuracy findings, evaluating the

DMD Fast Forward. Published on July 29, 2021 as DOI: 10.1124/dmd.121.000497
This article has not been copyedited and formatted. The final version may differ from this version.

data in this manner yielded similar conclusions with regard to the most appropriate input values used for in vivo [I]. If using organ entry concentrations, over-projection of the frequency of actual DDI was high, rendering the use of in vitro TDI essentially uninformative for such decision-making (Table 5). This observation was similar irrespective of the cutoff values used (1.25- or 2-fold). However, when organ exit concentrations were employed, the sensitivity remained high and the selectivity increased (fewer false positives). Method 4 with HLM data also yielded a mean fold error of 2.0-fold. Thus, the overall conclusion for static models is that the use of TDI data from HLM along with $C_{avg,u}$ values for [I] (Model 4) is the recommendation for an optimal strategy when employing in vitro data for clinical study planning for CYP3A based DDI caused by TDI.

Similar observations were made from the data entered into Simcyp modeling (Tables 6 and 7). Simcyp modeling offers a more sophisticated approach than simple equations that assume a single static in vivo concentration of inhibitor and substrate when estimating DDI. In Simcyp, concentrations are correctly assumed to be changing over time and this is accounted for when projecting the extent of CYP3A inactivation. Model performance characteristics for Simcyp were even better than Model 4. When performance was evaluated using the categorical criteria, Simcyp yielded no false negative outcomes for HLM TDI data however when employing TDI data from HHEP there were instances of false negative outcomes (Table 7). Thus, the overall conclusion for Simcyp modeling for CYP3A DDI caused by TDI is that the best in vitro input data is from HLM.

Reasons behind why there are differences between TDI parameters generated in HHEP vs. HLM, particularly k_{inact}, have not been determined. Corrections for $f_{u,mic}$ and $K_{p,uu}$ were made before making comparisons, removing these as possible factors. Various reasons can be speculated, such as the presence of conjugating enzyme activities present in HHEP but absent in HLM that could remove inactivating metabolites, or the existence of some unknown enzyme protection mechanism in HHEP that is absent in HLM. The catalytic cycle of P450 activity is complex and possesses steps wherein the process can be

DMD Fast Forward. Published on July 29, 2021 as DOI: 10.1124/dmd.121.000497
This article has not been copyedited and formatted. The final version may differ from this version.

uncoupled resulting in generation of reactive oxygen species without catalyzing metabolism of the substrate, and alteration of this cycle in one system vs. the other could yield differences in enzyme inactivation. Furthermore, it has been proposed that there are multiple phases of inactivation in TDI experiments and that a more sophisticated method of deriving in vitro values from these experiments is needed as compared to the manner in which the present data were processed (Yadav et al., 2018; Yadav et al., 2020). Preliminary data has been generated that shows that not only are k_{inact} values different in the two systems but that partition coefficients also differ (data on file). The partition coefficient is a measure of the ratio of the molecules of substrate consumed per molecule of enzyme inactivated and is an inherent biochemical property of an enzyme-inactivator pair. Thus, there appears to be a difference in the manner in which CYP3A behaves in the intact hepatocyte system vs. microsome incubations. Further efforts to understand these differences at a fundamental biochemical level are underway and will be reported in due course. The drugs assessed here have not been demonstrated to be clinical inducers. However, this does not preclude them from possessing in vitro induction potential. While the current analysis excludes in vitro induction parameters, work is ongoing to determine how in vitro induction may play a role in aligning compounds for which over predictions were observed.

Lastly, from the simplest basic and static models to more sophisticated and complex PBPK models, there is always a level of uncertainty that arises from the assumptions required for various in vivo input parameters (e.g. k_{deg}, f_m, F_g, $[I]_{in\ vivo}$, $K_{p,uu\ in\ vivo}$) and conceptual simplifications needed for modelling. Regarding the latter, it is necessary to simplify that the target organs liver and intestine are homogeneous compartments as opposed to the complex multicompartment tissues that they truly are. Furthermore, subcellular distribution of the inactivators and substrates is likely heterogeneous, which cannot be currently measured. Absorption is a more complex kinetic process than what has been addressed in the present treatment, and further work is planned to evaluate the impact of more complex and multiphasic absorption models driving in vivo input concentrations (e.g. the ADAM model in Simcyp). Finally, it must be appreciated that there is uncertainty and variability in important input parameters like k_{deg} for

DMD Fast Forward. Published on July 29, 2021 as DOI: 10.1124/dmd.121.000497
This article has not been copyedited and formatted. The final version may differ from this version.

CYP3A4 and F_g for midazolam and other substrates, among others, as well as the potential impact of the role for CYP3A5 in the metabolism of the substrates in vivo. As the science and knowledge around these factors continue to develop, re-evaluation and refinement of DDI prediction methods will be necessary. With the present state of knowledge, the approaches described here offer the best performance for predicting DDI for CYP3A time-dependent inactivators that can be currently achieved.

In conclusion, it has been demonstrated that TDI data for CYP3A generated in either HLM or HHEP can be used effectively to predict the magnitude of DDI and to make decisions regarding the need for clinical DDI studies. Data from HLM appears to perform better overall regarding not missing any DDI, whether using static or dynamic modeling, however, use of these data tended to yield more over-projection of DDI as compared to TDI data generated using HHEP. Key to the success in this endeavor is the selection of the most appropriate value for the in vivo concentration of the inactivator at the most important sites of action, the liver and intestine. Projected organ exit concentrations were best, and the use of maximum or average values can work, depending on the reagent used to generate the in vitro TDI data. PBPK modeling using the Simcyp module, wherein concentrations of the substrate and inhibitor are changing over time, performed well in predicting DDI.

ACKNOWLEDGEMENTS

We would like to thank Samantha Jordan and the scientists at York Bioanalytical Solutions for their contributions towards the generation of the binding data.

DMD Fast Forward. Published on July 29, 2021 as DOI: 10.1124/dmd.121.000497
This article has not been copyedited and formatted. The final version may differ from this version.

AUTHORSHIP CONTRIBUTIONS

Participated in research design: Tseng, Eng, Lin, Cerny, Goosen, Obach.

Conducted experiments: Tseng, Eng.

Performed data analysis: Tseng, Eng, Lin, Cerny, Tess, Goosen, Obach.

Wrote or contributed to the writing of the manuscript: Tseng, Eng, Lin, Cerny, Goosen, Obach.

DMD Fast Forward. Published on July 29, 2021 as DOI: 10.1124/dmd.121.000497
This article has not been copyedited and formatted. The final version may differ from this version.

REFERENCES

ACD/pKa version 14, Advanced Chemistry Development, Inc., Toronto, On, Canada, www.acdlabs.com, 2021.

Austin RP, Barton P, Cockroft SL, Wenlock MC, and Riley RJ (2002) The influence of nonspecific microsomal binding on apparent intrinsic clearance, and its prediction from physicochemical properties. *Drug Metab Dispos* **30:**1497-1503.

Backman JT, Olkkola KT, Aranko K, Himberg JJ, and Neuvonen PJ (1994) Dose of midazolam should be reduced during diltiazem and verapamil treatments. *Br J Clin Pharmacol* **37:**221-225.

BioByte cLogP, version 4.3, Biobyte Corp., Claremont, CA, USA, www.biobyte.com.

Brown HS, Ito K, Galetin A, and Houston JB (2005) Prediction of in vivo drug-drug interactions from in vitro data: impact of incorporating parallel pathways of drug elimination and inhibitor absorption rate constant. *Br J Clin Pharmacol* **60:**508-518.

Chen Y, Liu L, Monshouwer M, and Fretland AJ (2011) Determination of time-dependent inactivation of CYP3A4 in cryopreserved human hepatocytes and assessment of human drug-drug interactions. *Drug Metab Dispos* **39:**2085-2092.

Cheng Y-C and Prusoff WH (1973) Relationship between the inhibition constant (KI) and the concentration of inhibitor which causes 50 per cent inhibition (I50) of an enzymatic reaction. *Biochemical Pharmacology* **22:**3099-3108.

Cook CS, Berry LM, and Burton E (2004) Prediction of in vivo drug interactions with eplerenone in man from in vitro metabolic inhibition data. *Xenobiotica* **34:**215-228.

Di L, Breen C, Chambers R, Eckley ST, Fricke R, Ghosh A, Harradine P, Kalvass JC, Ho S, Lee CA, Marathe P, Perkins EJ, Qian M, Tse S, Yan Z, and Zamek-Gliszczynski MJ (2017) Industry Perspective on Contemporary Protein-Binding Methodologies: Considerations for Regulatory Drug-Drug Interaction and Related Guidelines on Highly Bound Drugs. *J Pharm Sci* **106:**3442-3452.

Dutreix C, Munarini F, Lorenzo S, Roesel J, and Wang Y (2013) Investigation into CYP3A4-mediated drug-drug interactions on midostaurin in healthy volunteers. *Cancer Chemother Pharmacol* **72:**1223-1234.

Einolf HJ, Lin W, Won CS, Wang L, Gu H, Chun DY, He H, and Mangold JB (2017) Physiologically Based Pharmacokinetic Model Predictions of Panobinostat (LBH589) as a Victim and Perpetrator of Drug-Drug Interactions. *Drug Metab Dispos* **45:**1304-1316.

Eng H, Tseng E, Cerny MA, Goosen TC, and Obach RS (2021) Cytochrome P450 3A Time-Dependent Inhibition Assays Are Too Sensitive for Identification of Drugs Causing Clinically Significant Drug-Drug Interactions: A Comparison of Human Liver Microsomes and Hepatocytes and Definition of Boundaries for Inactivation Rate Constants. *Drug Metab Dispos* **49:**442-450.

Ernest CS, 2nd, Hall SD, and Jones DR (2005) Mechanism-based inactivation of CYP3A by HIV protease inhibitors. *J Pharmacol Exp Ther* **312:**583-591.

Fahmi OA, Maurer TS, Kish M, Cardenas E, Boldt S, and Nettleton D (2008) A combined model for predicting CYP3A4 clinical net drug-drug interaction based on CYP3A4 inhibition, inactivation, and induction determined in vitro. *Drug Metab Dispos* **36:**1698-1708.

FDA (2005) Drug approval package: Vaprisol (conivaptan). FDA application NDA 021697. FDA Silver Springs, MD.

FDA (2011) Drug approval package: Victrelis (boceprevir). FDA application NDA 202258. FDA Silver Springs, MD.

FDA (2020) Clinical Drug Interaction Studies - Cytochrome P450 Enzyme- and Transporter-Mediated Drug Interactions Guidance for Industry. *Center for Drug Evaluation and Research (CDER), US Department of Health and Human Services Food and Drug Administration*.

Friedman EJ, Fraser IP, Wang YH, Bergman AJ, Li CC, Larson PJ, Chodakewitz J, Wagner JA, and Stoch SA (2011) Effect of different durations and formulations of diltiazem on the single-dose pharmacokinetics of midazolam: how long do we go? *J Clin Pharmacol* **51:**1561-1570.

Friedman H, Greenblatt DJ, Burstein ES, Scavone JM, Harmatz JS, and Shader RI (1988) Triazolam kinetics: interaction with cimetidine, propranolol, and the combination. *J Clin Pharmacol* **28:**228-233.

Fromm MF, Busse D, Kroemer HK, and Eichelbaum M (1996) Differential induction of prehepatic and hepatic metabolism of verapamil by rifampin. *Hepatology* **24:**796-801.

Galetin A, Burt H, Gibbons L, and Houston JB (2006) Prediction of time-dependent CYP3A4 drug-drug interactions: impact of enzyme degradation, parallel elimination pathways, and intestinal inhibition. *Drug Metab Dispos* **34:**166-175.

Galetin A, Gertz M, and Houston JB (2008) Potential role of intestinal first-pass metabolism in the prediction of drug-drug interactions. *Expert Opin Drug Metab Toxicol* **4:**909-922.

Galetin A, Gertz M, and Houston JB (2010) Contribution of intestinal cytochrome p450-mediated metabolism to drug-drug inhibition and induction interactions. *Drug Metab Pharmacokinet* **25:**28-47.

Garg V, Chandorkar G, Farmer HF, Smith F, Alves K, and van Heeswijk RP (2012) Effect of telaprevir on the pharmacokinetics of midazolam and digoxin. *J Clin Pharmacol* **52:**1566-1573.

Gertz M, Davis JD, Harrison A, Houston JB, and Galetin A (2008) Grapefruit juice-drug interaction studies as a method to assess the extent of intestinal availability: utility and limitations. *Curr Drug Metab* **9:**785-795.

Gorski JC, Jones DR, Haehner-Daniels BD, Hamman MA, O'Mara EM, Jr., and Hall SD (1998) The contribution of intestinal and hepatic CYP3A to the interaction between midazolam and clarithromycin. *Clin Pharmacol Ther* **64:**133-143.

Greenblatt DJ, von Moltke LL, Harmatz JS, Chen G, Weemhoff JL, Jen C, Kelley CJ, LeDuc BW, and Zinny MA (2003) Time course of recovery of cytochrome p450 3A function after single doses of grapefruit juice. *Clin Pharmacol Ther* **74:**121-129.

Grimm SW, Einolf HJ, Hall SD, He K, Lim HK, Ling KH, Lu C, Nomeir AA, Seibert E, Skordos KW, Tonn GR, Van Horn R, Wang RW, Wong YN, Yang TJ, and Obach RS (2009) The conduct of in vitro studies to address time-dependent inhibition of drug-metabolizing enzymes: a perspective of the pharmaceutical research and manufacturers of America. *Drug Metab Dispos* **37:**1355-1370.

Guengerich FP (1995) Human Cytochrome P450 Enzymes, in: *Cytochrome P450: Structure, Mechanism, and Biochemistry* (de Montellano PRO ed), pp 473-535, Springer US, Boston, MA.

Gurley B, Hubbard MA, Williams DK, Thaden J, Tong Y, Gentry WB, Breen P, Carrier DJ, and Cheboyina S (2006) Assessing the clinical significance of botanical supplementation on human cytochrome P450 3A activity: comparison of a milk thistle and black cohosh product to rifampin and clarithromycin. *J Clin Pharmacol* **46:**201-213.

Gurley BJ, Swain A, Hubbard MA, Hartsfield F, Thaden J, Williams DK, Gentry WB, and Tong Y (2008) Supplementation with goldenseal (Hydrastis canadensis), but not kava kava (Piper methysticum), inhibits human CYP3A activity in vivo. *Clin Pharmacol Ther* **83:**61-69.

Handel J, Ziegler G, Gemeinhardt A, Stuber H, Fischer C, and Klotz U (1988) Lack of effect of nitrendipine on the pharmacokinetics and pharmacodynamics of midazolam during steady state. *Br J Clin Pharmacol* **25:**243-250.

Ito K, Iwatsubo T, Kanamitsu S, Nakajima Y, and Sugiyama Y (1998) Quantitative prediction of in vivo drug clearance and drug interactions from in vitro data on metabolism, together with binding and transport. *Annu Rev Pharmacol Toxicol* **38:**461-499.

Jones DR, Gorski JC, Hamman MA, Mayhew BS, Rider S, and Hall SD (1999) Diltiazem inhibition of cytochrome P-450 3A activity is due to metabolite intermediate complex formation. *J Pharmacol Exp Ther* **290:**1116-1125.

Kanamitsu S, Ito K, and Sugiyama Y (2000) Quantitative prediction of in vivo drug-drug interactions from in vitro data based on physiological pharmacokinetics: use of maximum unbound concentration of inhibitor at the inlet to the liver. *Pharm Res* **17:**336-343.

Keefer CE, Kauffman GW, and Gupta RR (2013) Interpretable, probability-based confidence metric for continuous quantitative structure-activity relationship models. *J Chem Inf Model* **53:**368-383.

Kenny JR, Mukadam S, Zhang C, Tay S, Collins C, Galetin A, and Khojasteh SC (2012) Drug-drug interaction potential of marketed oncology drugs: in vitro assessment of time-dependent cytochrome P450 inhibition, reactive metabolite formation and drug-drug interaction prediction. *Pharm Res* **29:**1960-1976.

Kharasch ED, Hankins DC, Jubert C, Thummel KE, and Taraday JK (1999) Lack of single-dose disulfiram effects on cytochrome P-450 2C9, 2C19, 2D6, and 3A4 activities: evidence for specificity toward P-450 2E1. *Drug Metab Dispos* **27:**717-723.

Kirby BJ, Collier AC, Kharasch ED, Whittington D, Thummel KE, and Unadkat JD (2011) Complex drug interactions of HIV protease inhibitors 1: inactivation, induction, and inhibition of cytochrome P450 3A by ritonavir or nelfinavir. *Drug Metab Dispos* **39:**1070-1078.

Kivisto KT, Lamberg TS, Kantola T, and Neuvonen PJ (1997) Plasma buspirone concentrations are greatly increased by erythromycin and itraconazole. *Clin Pharmacol Ther* **62:**348-354.

Kivisto KT, Lamberg TS, and Neuvonen PJ (1999) Interactions of buspirone with itraconazole and rifampicin: effects on the pharmacokinetics of the active 1-(2-pyrimidinyl)-piperazine metabolite of buspirone. *Pharmacol Toxicol* **84:**94-97.

Kokudai M, Inui N, Takeuchi K, Sakaeda T, Kagawa Y, and Watanabe H (2009) Effects of statins on the pharmacokinetics of midazolam in healthy volunteers. *J Clin Pharmacol* **49:**568-573.

Lamberg TS, Kivisto KT, and Neuvonen PJ (1999) Lack of effect of terfenadine on the pharmacokinetics of the CYP3A4 substrate buspirone. *Pharmacol Toxicol* **84:**165-169.

Mahmood I and Sahajwalla C (1999) Clinical pharmacokinetics and pharmacodynamics of buspirone, an anxiolytic drug. *Clin Pharmacokinet* **36:**277-287.

Mao J, Johnson TR, Shen Z, and Yamazaki S (2013) Prediction of crizotinib-midazolam interaction using the Simcyp population-based simulator: comparison of CYP3A time-dependent inhibition between human liver microsomes versus hepatocytes. *Drug Metab Dispos* **41:**343-352.

Mao J, Mohutsky MA, Harrelson JP, Wrighton SA, and Hall SD (2011) Prediction of CYP3A-mediated drug-drug interactions using human hepatocytes suspended in human plasma. *Drug Metab Dispos* **39:**591-602.

Mao J, Mohutsky MA, Harrelson JP, Wrighton SA, and Hall SD (2012) Predictions of cytochrome P450-mediated drug-drug interactions using cryopreserved human hepatocytes: comparison of plasma and protein-free media incubation conditions. *Drug Metab Dispos* **40:**706-716.

Martin DE, Zussman BD, Everitt DE, Benincosa LJ, Etheredge RC, and Jorkasky DK (1997) Paroxetine does not affect the cardiac safety and pharmacokinetics of terfenadine in healthy adult men. *J Clin Psychopharmacol* **17:**451-459.

Mayhew BS, Jones DR, and Hall SD (2000) An in vitro model for predicting in vivo inhibition of cytochrome P450 3A4 by metabolic intermediate complex formation. *Drug Metab Dispos* **28:**1031-1037.

Mullins ME, Horowitz BZ, Linden DH, Smith GW, Norton RL, and Stump J (1998) Life-threatening interaction of mibefradil and beta-blockers with dihydropyridine calcium channel blockers. *JAMA* **280:**157-158.

O'Brien SG, Meinhardt P, Bond E, Beck J, Peng B, Dutreix C, Mehring G, Milosavljev S, Huber C, Capdeville R, and Fischer T (2003) Effects of imatinib mesylate (STI571, Glivec) on the pharmacokinetics of simvastatin, a cytochrome p450 3A4 substrate, in patients with chronic myeloid leukaemia. *Br J Cancer* **89:**1855-1859.

Obach RS, Walsky RL, and Venkatakrishnan K (2007) Mechanism-based inactivation of human cytochrome p450 enzymes and the prediction of drug-drug interactions. *Drug Metab Dispos* **35:**246-255.

Obach RS, Walsky RL, Venkatakrishnan K, Gaman EA, Houston JB, and Tremaine LM (2006) The utility of in vitro cytochrome P450 inhibition data in the prediction of drug-drug interactions. *J Pharmacol Exp Ther* **316:**336-348.

Olkkola KT, Aranko K, Luurila H, Hiller A, Saarnivaara L, Himberg JJ, and Neuvonen PJ (1993) A potentially hazardous interaction between erythromycin and midazolam. *Clin Pharmacol Ther* **53:**298-305.

Paine MF, Shen DD, Kunze KL, Perkins JD, Marsh CL, McVicar JP, Barr DM, Gillies BS, and Thummel KE (1996) First-pass metabolism of midazolam by the human intestine. *Clin Pharmacol Ther* **60:**14-24.

Prueksaritanont T, Ma B, Tang C, Meng Y, Assang C, Lu P, Reider PJ, Lin JH, and Baillie TA (1999) Metabolic interactions between mibefradil and HMG-CoA reductase inhibitors: an in vitro investigation with human liver preparations. *Br J Clin Pharmacol* **47:**291-298.

Prueksaritanont T, Tatosian DA, Chu X, Railkar R, Evers R, Chavez-Eng C, Lutz R, Zeng W, Yabut J, Chan GH, Cai X, Latham AH, Hehman J, Stypinski D, Brejda J, Zhou C, Thornton B, Bateman KP, Fraser I, and Stoch SA (2017) Validation of a microdose probe drug cocktail for clinical drug interaction assessments for drug transporters and CYP3A. *Clin Pharmacol Ther* **101:**519-530.

Quinney SK, Haehner BD, Rhoades MB, Lin Z, Gorski JC, and Hall SD (2008) Interaction between midazolam and clarithromycin in the elderly. *Br J Clin Pharmacol* **65:**98-109.

Riccardi K, Lin J, Li Z, Niosi M, Ryu S, Hua W, Atkinson K, Kosa RE, Litchfield J, and Di L (2017) Novel Method to Predict In Vivo Liver-to-Plasma Kpuu for OATP Substrates Using Suspension Hepatocytes. *Drug Metab Dispos* **45:**576-580.

Riccardi K, Ryu S, Lin J, Yates P, Tess D, Li R, Singh D, Holder BR, Kapinos B, Chang G, and Di L (2018) Comparison of Species and Cell-Type Differences in Fraction Unbound of Liver Tissues, Hepatocytes, and Cell Lines. *Drug Metab Dispos* **46:**415-421.

Ring BJ, Patterson BE, Mitchell MI, Vandenbranden M, Gillespie J, Bedding AW, Jewell H, Payne CD, Forgue ST, Eckstein J, Wrighton SA, and Phillips DL (2005) Effect of tadalafil on cytochrome P450 3A4-mediated clearance: studies in vitro and in vivo. *Clin Pharmacol Ther* **77:**63-75.

Rostami-Hodjegan A and Tucker G (2004) 'In silico' simulations to assess the 'in vivo' consequences of 'in vitro' metabolic drug-drug interactions. *Drug Discov Today Technol* **1:**441-448.

Rowland M and Matin SB (1973) Kinetics of drug-drug interactions. *Journal of Pharmacokinetics and Biopharmaceutics* **1:**553-567.

Rowland Yeo K, Walsky RL, Jamei M, Rostami-Hodjegan A, and Tucker GT (2011) Prediction of time-dependent CYP3A4 drug-drug interactions by physiologically based pharmacokinetic modelling: impact of inactivation parameters and enzyme turnover. *Eur J Pharm Sci* **43:**160-173.

Shou M, Hayashi M, Pan Y, Xu Y, Morrissey K, Xu L, and Skiles GL (2008) Modeling, prediction, and in vitro in vivo correlation of CYP3A4 induction. *Drug Metab Dispos* **36:**2355-2370.

Simcyp Certera Simcyp Library Files. https://members.simcyp.com/account/libraryFiles).

Tomalik-Scharte D, Jetter A, Kinzig-Schippers M, Skott A, Sorgel F, Klaassen T, Kasel D, Harlfinger S, Doroshyenko O, Frank D, Kirchheiner J, Brater M, Richter K, Gramatte T, and Fuhr U (2005) Effect of propiverine on cytochrome P450 enzymes: a cocktail interaction study in healthy volunteers. *Drug Metab Dispos* **33:**1859-1866.

Treyer A, Mateus A, Wisniewski JR, Boriss H, Matsson P, and Artursson P (2018) Intracellular Drug Bioavailability: Effect of Neutral Lipids and Phospholipids. *Mol Pharm* **15:**2224-2233.

Treyer A, Walday S, Boriss H, Matsson P, and Artursson P (2019) A Cell-Free Approach Based on Phospholipid Characterization for Determination of the Cell Specific Unbound Drug Fraction (fu,cell). *Pharm Res* **36:**178.

Wang YH, Jones DR, and Hall SD (2004) Prediction of cytochrome P450 3A inhibition by verapamil enantiomers and their metabolites. *Drug Metab Dispos* **32:**259-266.

Wang Z, Yang J, Kirk C, Fang Y, Alsina M, Badros A, Papadopoulos K, Wong A, Woo T, Bomba D, Li J, and Infante JR (2013) Clinical pharmacokinetics, metabolism, and drug-drug interaction of carfilzomib. *Drug Metab Dispos* **41:**230-237.

Yadav J, Korzekwa K, and Nagar S (2018) Improved Predictions of Drug-Drug Interactions Mediated by Time-Dependent Inhibition of CYP3A. *Mol Pharm* **15:**1979-1995.

Yadav J, Paragas E, Korzekwa K, and Nagar S (2020) Time-dependent enzyme inactivation: Numerical analyses of in vitro data and prediction of drug-drug interactions. *Pharmacol Ther* **206:**107449.

Yang J, Jamei M, Yeo KR, Rostami-Hodjegan A, and Tucker GT (2007a) Misuse of the well-stirred model of hepatic drug clearance. *Drug Metab Dispos* **35:**501-502.

Yang J, Jamei M, Yeo KR, Tucker GT, and Rostami-Hodjegan A (2007b) Prediction of intestinal first-pass drug metabolism. *Curr Drug Metab* **8:**676-684.

Yang J, Liao M, Shou M, Jamei M, Yeo KR, Tucker GT, and Rostami-Hodjegan A (2008) Cytochrome p450 turnover: regulation of synthesis and degradation, methods for determining rates, and implications for the prediction of drug interactions. *Curr Drug Metab* **9:**384-394.

Yates P, Eng H, Di L, and Obach RS (2012) Statistical methods for analysis of time-dependent inhibition of cytochrome p450 enzymes. *Drug Metab Dispos* **40:**2289-2296.

Yeates RA, Laufen H, and Zimmermann T (1996) Interaction between midazolam and clarithromycin: comparison with azithromycin. *Int J Clin Pharmacol Ther* **34:**400-405.

Zdravkovic M, Olsen AK, Christiansen T, Schulz R, Taub ME, Thomsen MS, Rasmussen MH, and Ilondo MM (2003) A clinical study investigating the pharmacokinetic interaction between NN703 (tabimorelin), a potential inhibitor of CYP3A4 activity, and midazolam, a CYP3A4 substrate. *Eur J Clin Pharmacol* **58:**683-688.

Zhang L, Reynolds KS, Zhao P, and Huang SM (2010) Drug interactions evaluation: an integrated part of risk assessment of therapeutics. *Toxicol Appl Pharmacol* **243:**134-145.

Zhou S, Chan E, Lim LY, Boelsterli UA, Li SC, Wang J, Zhang Q, Huang M, and Xu A (2004) Therapeutic drugs that behave as mechanism-based inhibitors of cytochrome P450 3A4. *Curr Drug Metab* **5:**415-442.

Zhou SF (2008) Drugs behave as substrates, inhibitors and inducers of human cytochrome P450 3A4. *Curr Drug Metab* **9:**310-322.

Zimmerlin A, Trunzer M, and Faller B (2011) CYP3A time-dependent inhibition risk assessment validated with 400 reference drugs. *Drug Metab Dispos* **39:**1039-1046.

Zimmermann T, Yeates RA, Laufen H, Scharpf F, Leitold M, and Wildfeuer A (1996) Influence of the antibiotics erythromycin and azithromycin on the pharmacokinetics and pharmacodynamics of midazolam. *Arzneimittelforschung* **46:**213-217.

Footnotes

Financial Disclosure: This work received no external funding.

Declaration of interest: The authors are employees of Pfizer and report no conflicts of interest. The authors alone are responsible for the content and writing of the paper.

Address correspondence to:

Elaine Tseng, Pfizer Inc., Eastern Point Rd, Groton, CT 06340. E-mail: elaine.tseng@pfizer.com; or

R. Scott Obach, Pfizer Inc., Eastern Point Rd, Groton, CT 06340. E-mail: r.scott.obach@pfizer.com.

DMD Fast Forward. Published on July 29, 2021 as DOI: 10.1124/dmd.121.000497
This article has not been copyedited and formatted. The final version may differ from this version.

FIGURE LEGENDS

Figure 1. Comparison of TDI parameters obtained in liver microsomes (HLM) vs hepatocytes (HHEP). Panel A: $K_{I,u}$; Panel B: k_{inact}; and Panel C: $k_{inact}/K_{I,u}$. Solid black lines represent unity and dotted lines represent 2-fold and 3-fold deviation from unity, and solid red line represents bias. Azithromycin, nelfinavir, terfenadine, paroxetine, and eplerenone are not shown in panels A and B because individual K_I and k_{inact} were not able to be determined.

Figure 2. Predicted vs Observed AUC ratios from mechanistic static Model 4 (Panels A & B) and Simcyp modeling (Panels C & D).

Panels A and C are results using human liver microsome-generated inactivation parameters and Panels B and D are results human hepatocyte-generated inactivation parameters. Solid black lines represent unity, dotted lines represent 2-fold and 3-fold deviation from unity, and red solid lines represent the bias.

Figure 3. Model performance versus observed AUCR from mechanistic static Model 4 (Panels A & B) and Simcyp modeling (Panels C & D).

Panels A and C are results using human liver microsome-generated inactivation parameters and Panels B and D are results human hepatocyte-generated inactivation parameters. Shaded green area represents 0.5- to 2-fold criteria. Pro, propranolol; Tad, tadalafil; Nit, nitrendipine; Epl, eplerenone; Par, paroxetine; Mid, midostaurin; Pan, Panobinostat; Dis, disulfiram; Car, carfilzomib; Ter, terfenadine; Azi, azithromycin; Sim, simvastatin; Ppv, propiverine; Nel IV, nelfinavir (IV midazolam); Tab, tabimorelin; Ima, imatinib; Ver, verapamil; Dil, diltiazem; Ery, erythromycin; Tel IV; telaprevir (IV midazolam); Boc, boceprevir; Con, conivaptan; Cla, clarithromycin; Tel, telaprevir

DMD Fast Forward. Published on July 29, 2021 as DOI: 10.1124/dmd.121.000497
This article has not been copyedited and formatted. The final version may differ from this version.

Figure 4. Classification of predicted (Pred) AUCR versus observed (Obs) AUCR using 1.25- and 2-fold cutoff criteria in mechanistic static models 1-4.

Values in each section of the bar graphs represent the number of drugs that were predicted to be true positives (TP), true negatives (TN), false positives (FP), or false negatives (FN) using liver microsome (panel A) or hepatocyte- (panel B) generated parameters.

Figure 5. Classification of predicted (Pred) AUCR versus observed (Obs) AUCR using 1.25- and 2-fold cutoff criteria using Simcyp.

Values in each section of the bar graphs represent the number of drugs that were predicted to be true positives (TP), true negatives (TN), false positives (FP), or false negatives (FN) using liver microsome (HLM) or hepatocyte- (HHEP) generated parameters.

Figure 6. Correlation of predicted AUC ratios (AUCR) from mechanistic static Model 4 and Simcyp modeling.

Panel A represents predictions using human liver microsome-generated inactivation parameters and Panel B represents predictions using human hepatocyte-generated inactivation parameters. The solid black line represents unity.

Table 1. Summary of observed clinical drug-drug interactions for CYP3A cleared drugs.

Drug Name	Inhibitor Dose	Substrate Dose[b]	Clinical Interaction (AUCR)	Clinical Interaction Reference
Azithromycin	500 mg QD; 3d	15 mg PO midazolam	1.23[a]	(Yeates et al., 1996; Zimmermann et al., 1996)
Boceprevir	800 mg TID, 6d	4 mg PO midazolam	5.05	(FDA, 2011)
Carfilzomib	27 mg/m2, IV, various	2 mg PO midazolam	1.10	(Wang et al., 2013)
Clarithromycin	500 mg BID; 7d	4 mg PO midazolam	6.69[a]	(Gorski et al., 1998; Gurley et al., 2006; Gurley et al., 2008; Quinney et al., 2008; Prueksaritanont et al., 2017)
Conivaptan	40 mg BID, 5d	2 mg PO midazolam[c]	5.76	(FDA, 2005)
Diltiazem	60 mg TID; 2d	2 mg PO midazolam	3.93[a]	(Backman et al., 1994; Friedman et al., 2011)
Disulfiram	500 mg single	1 mg IV midazolam	1.05	(Kharasch et al., 1999)
Eplerenone	100 mg QD; 6d	10 mg PO midazolam	0.96	(Cook et al., 2004)
Erythromycin	500 mg TID; 7d	4 mg PO midazolam	4.12[a]	(Olkkola et al., 1993; Zimmermann et al., 1996)
Imatinib	400 mg QD, 7d	40 mg PO simvastatin	2.92	(O'Brien et al., 2003)
Midostaurin	100 mg single dose	4 mg PO midazolam	1.00	(Dutreix et al., 2013)
Nelfinavir	1250 BID, 14d	2 mg PO midazolam	4.29[a]	(Kirby et al., 2011)
		1 mg IV midazolam	1.83	
Nitrendipine	20 mg single dose	0.07 mg/kg IV plus infusion midazolam	0.93 change in CL	(Handel et al., 1988)
Panobinostat	20 mg every other day; 15d	5 mg PO midazolam	1.04	(Einolf et al., 2017)
Paroxetine	20 mg QD; 15d	60 mg PO terfenadine[d]	0.97	(Martin et al., 1997)
Propiverine	15 mg BID, 7d	2 mg PO midazolam	1.46	(Tomalik-Scharte et al., 2005)
Propranolol	40 mg QD, 2d	0.5 mg PO triazolam	0.89	(Friedman et al., 1988)
Simvastatin	10 mg QD, 14d	15 ug/kg PO midazolam	1.24	(Kokudai et al., 2009)
Tabimorelin	3 mg/kg PO, 7d	7.5 mg PO midazolam	1.93	(Zdravkovic et al., 2003)
Tadalafil	10 mg QD, 14d	15 mg PO midazolam	0.90	(Ring et al., 2005)
Telaprevir	750 mg TID, 16d	2 mg PO midazolam	13.50	(Garg et al., 2012)
		0.5mg IV midazolam	4.92	
Terfenadine	120 mg QD, 3d	10 mg PO buspirone	1.19	(Lamberg et al., 1999)
Verapamil	80 mg TID, 2d	15 mg PO midazolam	2.92	(Backman et al., 1994)

[a]AUCR was calculated as a weighted average AUCR based on number of subjects in each study at the same dose per route (equation 1).

[b]substate (single dose) was given at the final day of inhibitor dose.

[c]substrate (QD), 5 days.

[d]substrate (BID), days 8 to 15, 8 days.

QD, once a day; BID, twice a day; TID, three times a day; IV, intravenous; PO, oral

Table 2. Total and free inhibition parameters determined in human liver microsomes.

Drug Name	Reversible Inhibition			Time-dependent Inhibition				
	K_i[a] (μM)	$f_{u,mic}$ (0.01 mg/mL)[d]	$K_{i,u}$ (μM)	K_I (SE) (μM)	$f_{u,mic}$ (%CV) (0.3 mg/mL)	$K_{I,u}$ (μM)	k_{inact} (SE) (min^{-1})	$k_{inact}/K_{I,u}$ ($mL \cdot min^{-1} \cdot \mu mol^{-1}$)
Azithromycin	>50.0	0.982	>49.1	NR	0.650 (9%)	NR	NR	0.025
Boceprevir	11.9	0.990	11.8	13.8 (1.7)	0.766 (12%)	10.6	0.304 (0.010)	28.8
Carfilzomib	2.19	0.964	2.11	1.18 (0.22)	0.473[b]	0.558	0.107 (0.007)	192
Clarithromycin	43.9	0.982	43.1	55.9 (13.4)	0.647 (16%)	36.2	0.0812 (0.0086)	2.25
Conivaptan	4.14	0.929	3.84	1.04 (0.16)	0.303 (4%)	0.315	0.329 (0.013)	1040
Diltiazem	20.3	0.986	20.0	1.90 (0.28)	0.696 (9%)	1.32	0.0109 (0.0004)	8.24
n-desmethyl Diltiazem[c]	ND	ND	ND	0.961 (0.115)	ND	0.961	0.00954 (0.00027)	9.94
Disulfiram[c]	1.18	ND	1.18	16.4 (5.2)	ND	16.4	0.129 (0.012)	7.87
Eplerenone	>50.0	0.991	>49.5	202 (58)	0.779 (10%)	157	0.0223 (0.0029)	0.142
Erythromycin	32.0	0.979	31.3	23.3 (3.3)	0.613 (38%)	14.3	0.0557 (0.0025)	3.90
Imatinib	28.9	0.974	28.2	16.4 (4.9)	0.560 (15%)	9.18	0.0348 (0.0029)	3.79
Midostaurin	2.79	0.267	0.740	0.360 (0.120)	0.0118 (29%)	0.00425	0.0207 (0.0015)	4870
Nelfinavir	1.46	0.561	0.816	1.44 (0.45)	0.0408 (21%)	0.0588	0.510 (0.057)	8680
Nitrendipine	1.37	0.960	1.32	10.4 (3.1)	0.444 (22%)	4.62	0.0266 (0.0020)	5.76
Panobinostat	4.99	0.971	4.84	30.3 (6.8)	0.530 (9%)	16.1	0.0436 (0.0027)	2.71
Paroxetine	13.4	0.833	11.2	49.4 (22.0)	0.143 (17%)	7.06	0.0277 (0.0084)	3.92
Propiverine	8.05	0.961	7.74	1.71 (0.23)	0.451 (25%)	0.771	0.0298 (0.0012)	38.7
Propranolol	>50.0	0.978	>48.9	No TDI	0.594 (3%)	No TDI	No TDI	No TDI

Simvastatin	0.146	0.651	0.095	NR	0.0585 (12%)	NR	NR	0.195
Tabimorelin	8.30	0.973	8.08	1.98 (0.31)	0.547 (12%)	1.08	0.0652 (0.0123)	60.2
Tadalafil	8.55	0.990	8.46	13.0 (1.7)	0.776 (4%)	10.1	0.143 (0.004)	14.2
Telaprevir	11.6	0.992	11.5	0.644 (0.109)	0.806 (9%)	0.519	0.108 (0.004)	208
Terfenadine	0.218	0.559	0.122	9.32 (5.85)	0.0405 (3%)	0.377	0.0276 (0.0111)	73.2
Verapamil	12.9	0.979	12.6	2.80 (0.54)	0.610 (23%)	1.71	0.0487 (0.0123)	28.5

[a] Calculated as measured $IC_{50}/2$.

[b] Based on in silico modeling.

[c] Total values were reported since unbound fractions were not determined.

[d] $f_{u,mic}$ was calculated from $f_{u,mic}$ measured at 0.3 mg/mL (n=3-4) using equation from (Austin et al., 2002).

%CV, percent coefficient of variation; SE, standard error; ND, not determined (assume 1); NR, not reported (see data analysis section for the estimation of $k_{inact}/K_{I,u}$)

Table 3. Total and free inhibition parameters determined in human hepatocytes**.**

Drug Name	Reversible Inhibition			Time-dependent Inhibition			
	K_i[a] (μM)	$K_{p,uu}$[b] (%CV)	$K_{i,u}$ (μM)	K_I (SE) (μM)	$K_{I,u}$ (μM)	k_{inact} (SE) (min^{-1})	$k_{inact}/K_{I,u}$ ($mL \cdot min^{-1} \cdot \mu mol^{-1}$)
Azithromycin	>25.0	5.70 (5%)	>143	51.2 (17.3)	292	0.0327 (0.0032)	0.112
Boceprevir	10.8	0.190 (0.5%)	2.04	25.9 (10.7)	4.92	0.0978 (0.0161)	19.9
Carfilzomib	1.71	0.0160 (33%)	0.0300	7.76 (2.26)	0.126	0.0289 (0.0020)	229
Clarithromycin	13.8	0.600 (7%)	8.25	7.45 (2.06)	4.47	0.0112 (0.0007)	2.51
Conivaptan	1.27	1.70 (8%)	2.16	0.634 (0.124)	1.08	0.0182 (0.0010)	16.9
Diltiazem	13.0	0.253 (10%)	3.28	35.4 (6.6)	8.96	0.0217 (0.0010)	2.42
n-desmethyl Diltiazem[c]	ND	ND	ND	2.96 (1.12)	2.96	0.0127 (0.0011)	4.29
Disulfiram	ND	ND	ND	ND	ND	ND	ND
Eplerenone	>25.0	0.141 (13%)	>3.53	NR	NR	NR	0.0166
Erythromycin	16.9	0.328 (9%)	5.06	27.1 (19.7)	8.13	0.0141 (0.0044)	1.73
Imatinib	22.5	1.00 (16%)	22.5	29.4 (8.1)	29.4	0.0202 (0.0014)	0.687
Midostaurin	>25.0	0.005 (43%)	>0.120	0.574 (0.165)	0.00276	0.00566 (0.00041)	2050
Nelfinavir	0.496	1.70 (12%)	0.842	NR	NR	NR	6.24
Nitrendipine	ND	ND	ND	ND	ND	ND	ND
Panobinostat	>25.0	0.600 (11%)	>15.0	26.0 (7.2)	15.6	0.00446 (0.00038)	0.286
Paroxetine	14.3	0.600 (14%)	8.55	NR	NR	NR	0.113

Propiverine	7.50	0.500 (15%)	3.75	1.38 (0.62)	0.690	0.0196 (0.0040)	28.4
Propranolol	ND	ND	ND	ND	ND	ND	ND
Simvastatin	ND	ND	ND	ND	ND	ND	ND
Tabimorelin	2.85	0.200 (18%)	0.569	7.57 (2.62)	1.51	0.0148 (0.0013)	9.78
Tadalafil	12.9	0.600 (5%)	7.71	4.26 (1.44)	2.56	0.028 (0.002)	11.0
Telaprevir	0.273	0.450 (17%)	0.123	2.24 (0.95)	1.01	0.0112 (0.0011)	11.1
Terfenadine	2.17	1.40	3.04	NR	NR	NR	0.426
Verapamil	13.4	0.310 (20%)	4.14	0.661 (0.143)	0.205	0.0172 (0.0010)	83.9

[a]Calculated as measured $IC_{50}/2$.

[b]Calculated from K_p (n=3) and $f_{u,liver}$ reported in supplemental tables.

[c]Total value was reported since $K_{p,uu}$ was not determined.

%CV, percent coefficient of variation; SE, standard error; ND, not determined since no TDI was detected in a single concentration screen at 30 µM; NR, not reported see data analysis section for the estimation of $k_{inact}/K_{I,u}$

DMD Fast Forward. Published on July 29, 2021 as DOI: 10.1124/dmd.121.000497
This article has not been copyedited and formatted. The final version may differ from this version.

Table 4. Numerical accuracy of DDI predictions determined from human liver microsomes and human hepatocytes using mechanistic static models**.**

	Model 1	**Model 2**	**Model 3**	**Model 4**
Relevant $[I]_{gut}$	entrance	entrance	exit	exit
Relevant $[I]_{liver}$	entrance	entrance	exit	exit
		Fixed Input Parameters		
F_a		1		
CYP3A $k_{deg,g}$		0.00050 min^{-1}		
CYP3A $k_{deg,h}$		0.00032 min^{-1}		
Q_g	300 mL/min	300 mL/min	1213 mL/min	1213 mL/min
Q_h	1617 mL/min	1617 mL/min	NA	NA
		Varied Input Parameters		
k_a	0.1 min^{-1}	custom	custom	custom
$[I]_g$	Total Enterocyte[a]	Free Enterocyte[b]	$C_{max,portal,u}$[c]	$C_{avg,portal,u}$[d]
$[I]_h$	$C_{max,hepatic\ inlet,u}$[e]	$C_{max,hepatic\ inlet,u}$[e]	$C_{max,systemic,u}$	$C_{avg,systemic,u}$
$f_{u,gut}$	1	$f_{u,plasma}$	$f_{u,plasma}$	$f_{u,plasma}$
Performance:		**Human Liver Microsomes**		
Bias ($CI_{90\%}$)	6.3 (4.8-8.1)	5.0 (3.8-6.5)	2.7 (2.2-3.4)	1.8 (1.5-2.3)
GMFE ($CI_{90\%}$)	6.3 (4.8-8.1)	5.1 (3.9-6.6)	2.8 (2.3-3.5)	2.0 (1.6-2.4)
RMSFE	7.38	6.09	3.37	2.42
% Within 2-fold	12	12	36	56
% Within 3-fold	16	28	48	80
% Outside 10-fold	24	16	4	0
Performance:		**Human Hepatocytes**		
Bias ($CI_{90\%}$)	3.8 (2.9-4.9)	2.7 (2.0-3.4)	1.6 (1.2-2.1)	1.1 (0.88-1.4)
GMFE ($CI_{90\%}$)	3.8 (3.0-4.9)	2.7 (2.1-3.5)	2.0 (1.6-2.5)	1.7 (1.4-2.0)
RMSFE	4.70	3.49	2.52	2.04
% Within 2-fold	24	44	56	68
% Within 3-fold	36	60	76	84
% Outside 10-fold	12	4	0	0

[a]As calculated per equation 7a.

[b]As calculated per equation 7a corrected for free fraction in plasma.

[c]As calculated per equation 7b.

[d]As calculated per equation 7c.

[e]As calculated per equation 6.

NA, not applicable; $[I]_g$, intestinal inhibitor concentration; $[I]_h$, liver inhibitor concentration; F_a, fraction absorbed following oral dose; $k_{deg,g}$, intestinal degradation rate; $k_{deg,h}$, hepatic degradation rate; Q_g, intestinal blood flow; Q_h, liver blood flow; k_a, inhibitor absorption rate constant; $f_{u,gut}$, intestinal free fraction; $f_{u,plasma}$, plasma free fraction; $C_{max,portal,u}$, unbound maximum portal concentration; $C_{max,systemic,u}$ unbound maximum systemic concentration; $C_{avg,systemic,u}$, unbound average systemic concentration; GMFE, geometric mean fold error; CI90%, 90% confidence interval; RMSFE, root mean square fold error

DMD Fast Forward. Published on July 29, 2021 as DOI: 10.1124/dmd.121.000497
This article has not been copyedited and formatted. The final version may differ from this version.

Table 5: Categorical accuracy of DDI predictions using mechanistic static models.

DDI Cutoff	Matrix	Model	N	Sensitivity (%)	Specificity (%)	PPV (%)	NPV (%)	PPE (%)	NPE (%)
Clinical ≥1.25-fold & Prediction ≥1.25-fold	Human Liver Microsomes	1	25	100	8	54	100	46	0
		2	25	100	17	57	100	43	0
		3	25	100	25	59	100	41	0
		4	25	100	67	76	100	24	0
	Human Hepatocytes	1	25	100	33	62	100	38	0
		2	25	100	33	62	100	38	0
		3	25	100	58	72	100	28	0
		4	25	92	67	75	89	25	11
Clinical ≥2-fold & Prediction ≥2-fold	Human Liver Microsomes	1	25	100	13	43	100	57	0
		2	25	100	13	43	100	57	0
		3	25	100	33	50	100	50	0
		4	25	100	67	67	100	33	0
	Human Hepatocytes	1	25	100	27	48	100	52	0
		2	25	100	40	53	100	47	0
		3	25	90	67	64	91	36	9
		4	25	70	80	70	80	30	20

PPV, positive predictive value; NPR, negative predictive value; PPE, positive predictive error; NPE, negative predictive error

DMD Fast Forward. Published on July 29, 2021 as DOI: 10.1124/dmd.121.000497
This article has not been copyedited and formatted. The final version may differ from this version.

Table 6: Numerical accuracy of DDI predictions using Simcyp

Performance:	Human Liver Microsomes	Human Hepatocytes
Bias (CI90%)	1.6 (1.3-1.9)	1.1 (0.85-1.3)
GMFE (CI90%)	1.7 (1.5-2.0)	1.6 (1.4-1.8)
RMSFE	2.02	1.88
% Within 2-fold	64	68
% Within 3-fold	88	88
% Outside 10-fold	0	0

GMFE, geometric mean fold error; RMSFE, root mean square fold error

DMD Fast Forward. Published on July 29, 2021 as DOI: 10.1124/dmd.121.000497
This article has not been copyedited and formatted. The final version may differ from this version.

Table 7: Categorical accuracy DDI predictions using Simcyp

DDI Cutoff	Matrix	N	Sensitivity (%)	Specificity (%)	PPV (%)	NPV (%)	PPE (%)	NPE (%)
Clinical ≥1.25-fold & Prediction	Human Liver Microsomes	25	100	67	76	100	24	0
	Human Hepatocytes	25	85	83	85	83	15	17
Clinical ≥2-fold & Prediction	Human Liver Microsomes	25	100	80	77	100	23	0
	Human Hepatocytes	25	70	80	70	80	30	20

PPV, positive predictive value; NPR, negative predictive value; PPE, positive predictive error; NPE, negative predictive error

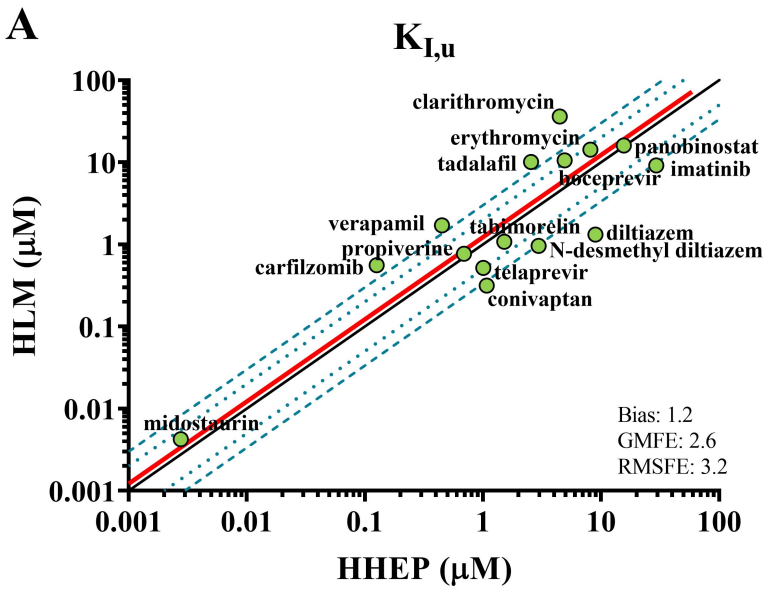
A
$K_{I,u}$
clarithromycin
erythromycin
panobinostat
tadalafil
boceprevir
imatinib
verapamil
tabimorelin
diltiazem
propiverine
N-desmethyl diltiazem
carfilzomib
telaprevir
conivaptan
midostaurin
Bias: 1.2
GMFE: 2.6
RMSFE: 3.2
HLM (μM)
HHEP (μM)
100
10
1
0.1
0.01
0.001
0.001
0.01
0.1
1
10
100

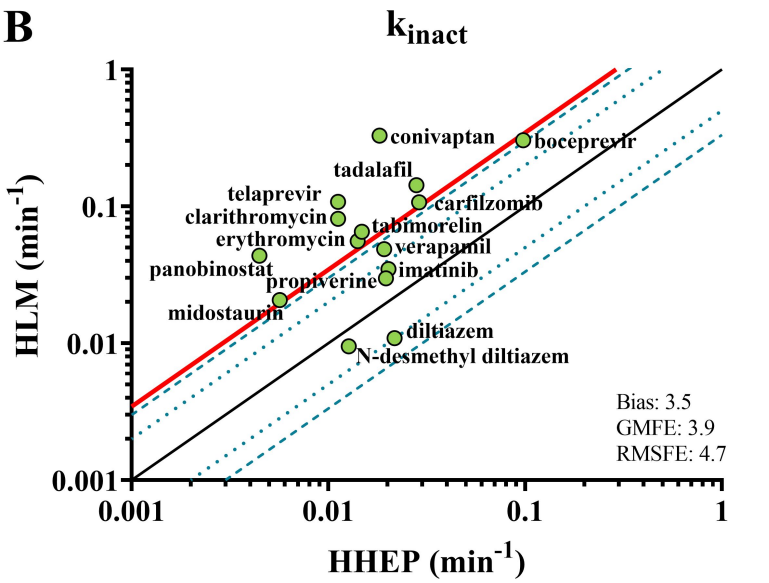
B
k_{inact}
conivaptan
boceprevir
tadalafil
telaprevir
carfilzomib
clarithromycin
tabimorelin
erythromycin
verapamil
panobinostat
imatinib
propiverine
midostaurin
diltiazem
N-desmethyl diltiazem
Bias: 3.5
GMFE: 3.9
RMSFE: 4.7
HLM (min^{-1})
HHEP (min^{-1})
1
0.1
0.01
0.001
0.001
0.01
0.1
1

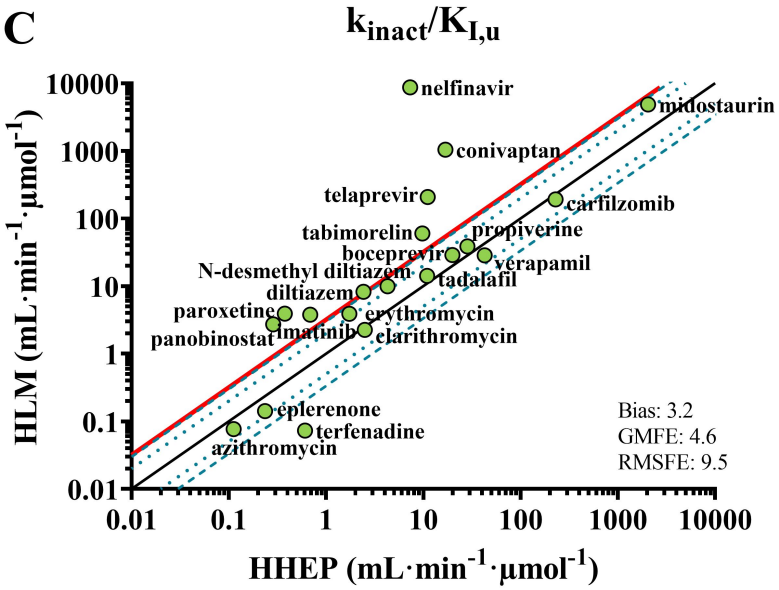
C
$k_{inact}/K_{I,u}$
nelfinavir
midostaurin
conivaptan
telaprevir
carfilzomib
tabimorelin
propiverine
boceprevir
verapamil
N-desmethyl diltiazem
tadalafil
diltiazem
paroxetine
erythromycin
panobinostat
imatinib
clarithromycin
eplerenone
terfenadine
azithromycin
Bias: 3.2
GMFE: 4.6
RMSFE: 9.5
HLM ($mL \cdot min^{-1} \cdot \mu mol^{-1}$)
HHEP ($mL \cdot min^{-1} \cdot \mu mol^{-1}$)
10000
1000
100
10
1
0.1
0.01
0.01
0.1
1
10
100
1000
10000

Figure 1

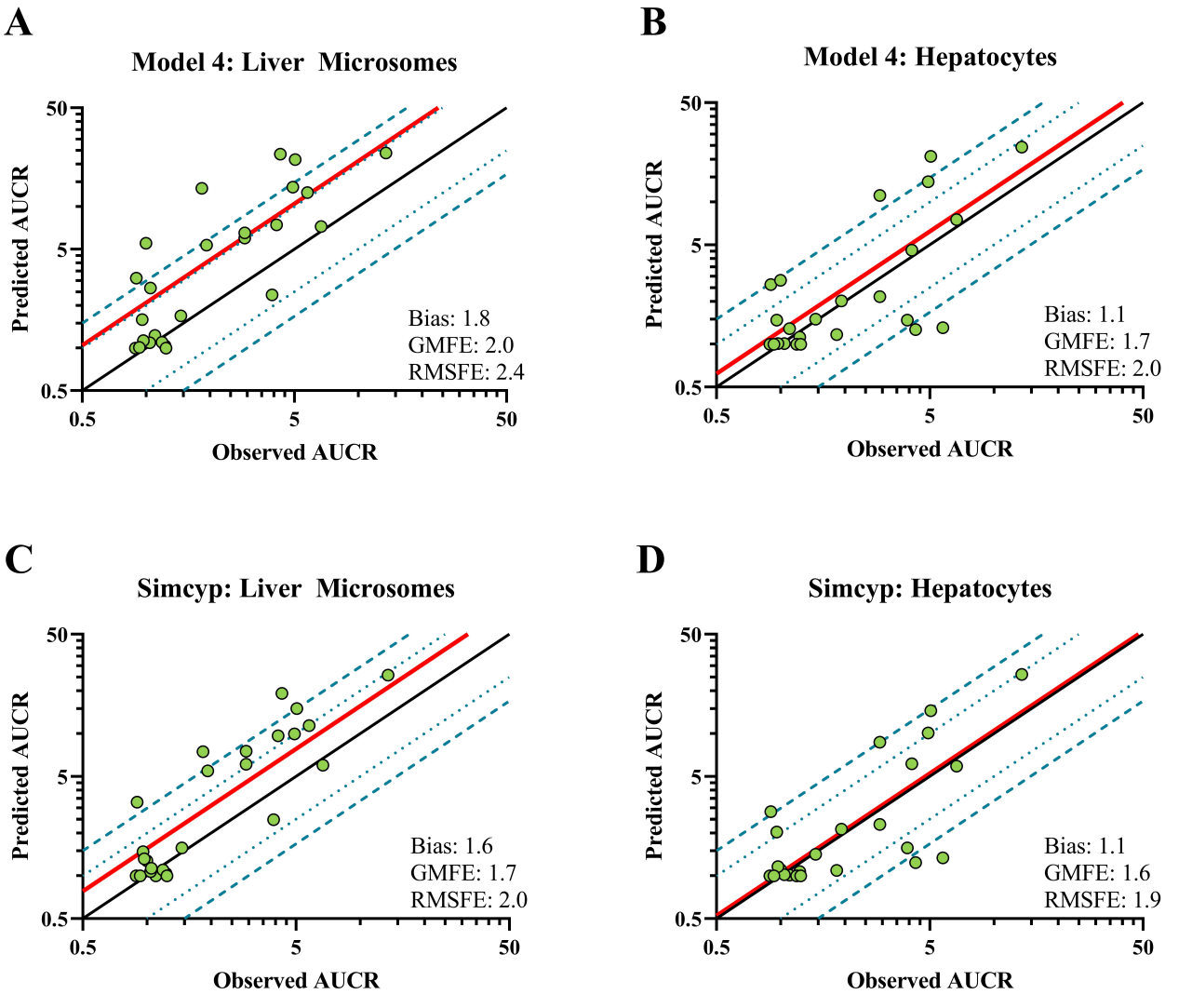
A
Model 4: Liver Microsomes
Predicted AUCR
Observed AUCR
0.5
5
50
Bias: 1.8
GMFE: 2.0
RMSFE: 2.4
B
Model 4: Hepatocytes
Bias: 1.1
GMFE: 1.7
RMSFE: 2.0
C
Simcyp: Liver Microsomes
Bias: 1.6
GMFE: 1.7
RMSFE: 2.0
D
Simcyp: Hepatocytes
Bias: 1.1
GMFE: 1.6
RMSFE: 1.9

Figure 2

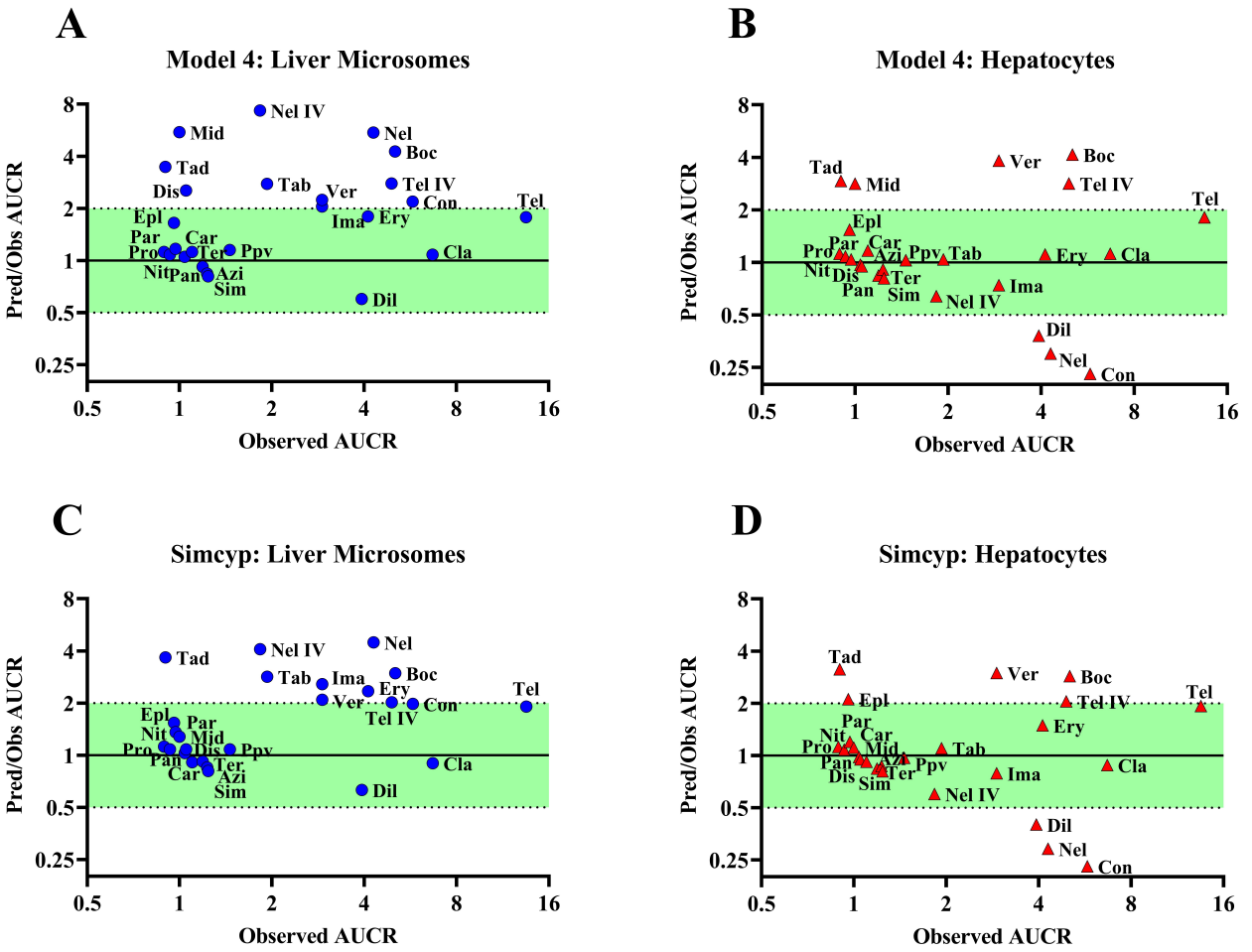
A
Model 4: Liver Microsomes
Pred/Obs AUCR
Observed AUCR
Nel IV
Mid
Nel
Boc
Tad
Tab
Ver
Tel IV
Dis
Con
Tel
Epl
Ima
Ery
Par
Car
Pro
Ter
Ppv
Cla
Nit
Pan
Azi
Sim
Dil
B
Model 4: Hepatocytes
Pred/Obs AUCR
Observed AUCR
Tad
Ver
Boc
Mid
Tel IV
Tel
Epl
Par
Car
Pro
Azi
Ppv
Tab
Ery
Cla
Nit
Dis
Ter
Pan
Sim
Ima
Nel IV
Dil
Nel
Con
C
Simcyp: Liver Microsomes
Pred/Obs AUCR
Observed AUCR
Tad
Nel IV
Nel
Tab
Ima
Boc
Ery
Tel
Ver
Con
Epl
Tel IV
Par
Nit
Mid
Pro
Dis
Ppv
Pan
Ter
Cla
Car
Azi
Sim
Dil
D
Simcyp: Hepatocytes
Pred/Obs AUCR
Observed AUCR
Tad
Ver
Boc
Tel
Epl
Tel IV
Par
Ery
Nit
Car
Pro
Mid
Tab
Pan
Azi
Ppv
Ter
Cla
Dis
Sim
Ima
Nel IV
Dil
Nel
Con

Figure 3

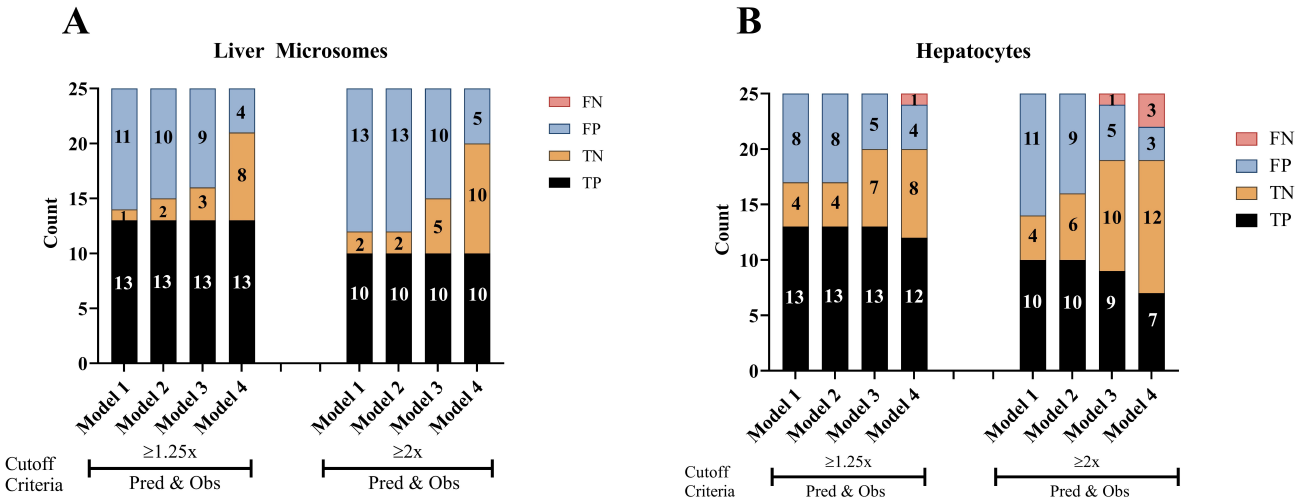
A
Liver Microsomes
B
Hepatocytes
Count
FN
FP
TN
TP
Model 1
Model 2
Model 3
Model 4
Cutoff Criteria
≥1.25x
≥2x
Pred & Obs

Figure 4

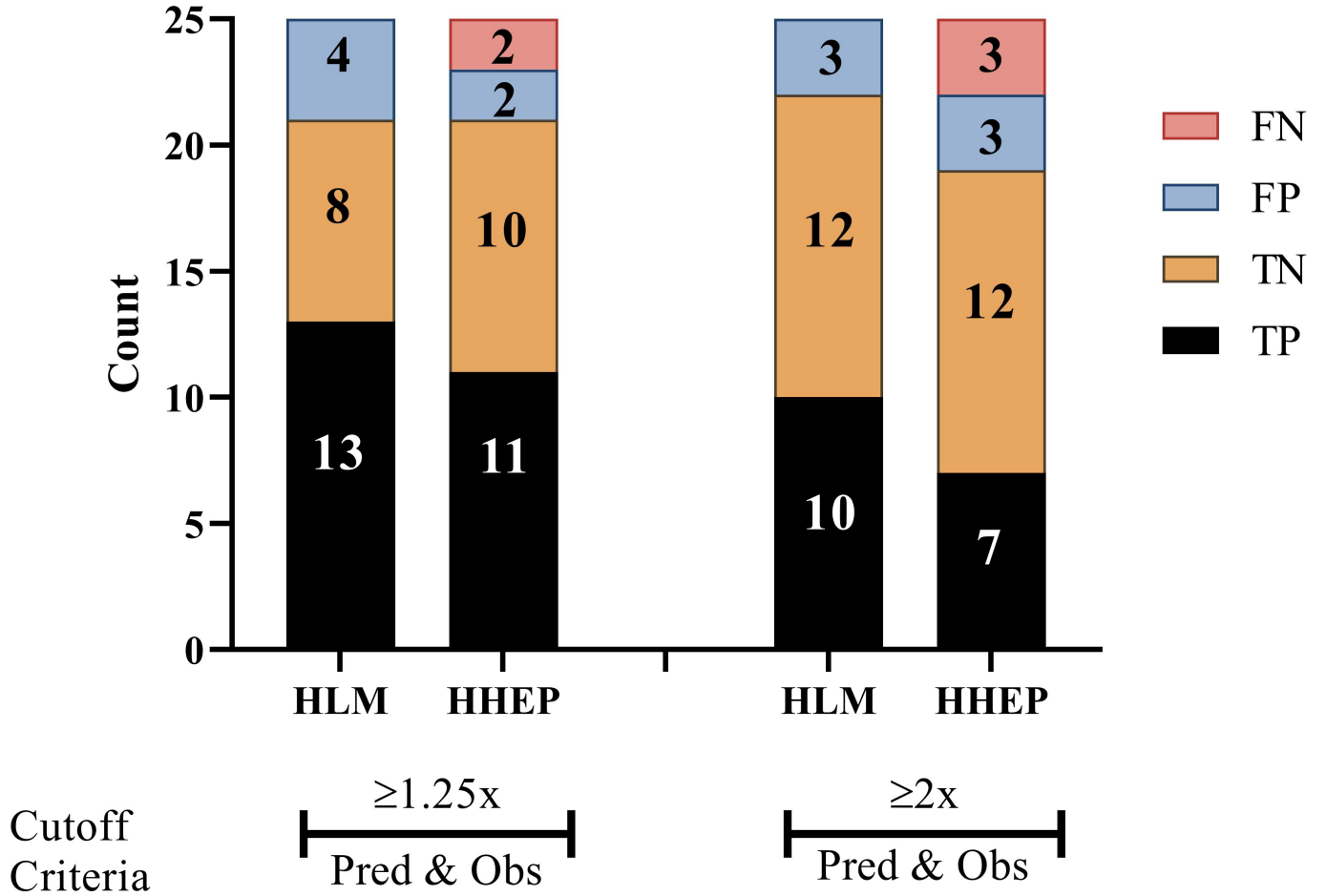
25
20
15
10
5
0
Count
4
8
13
2
2
10
11
3
12
10
3
3
12
7
FN
FP
TN
TP
HLM
HHEP
HLM
HHEP
Cutoff
Criteria
≥1.25x
Pred & Obs
≥2x
Pred & Obs

Figure 5

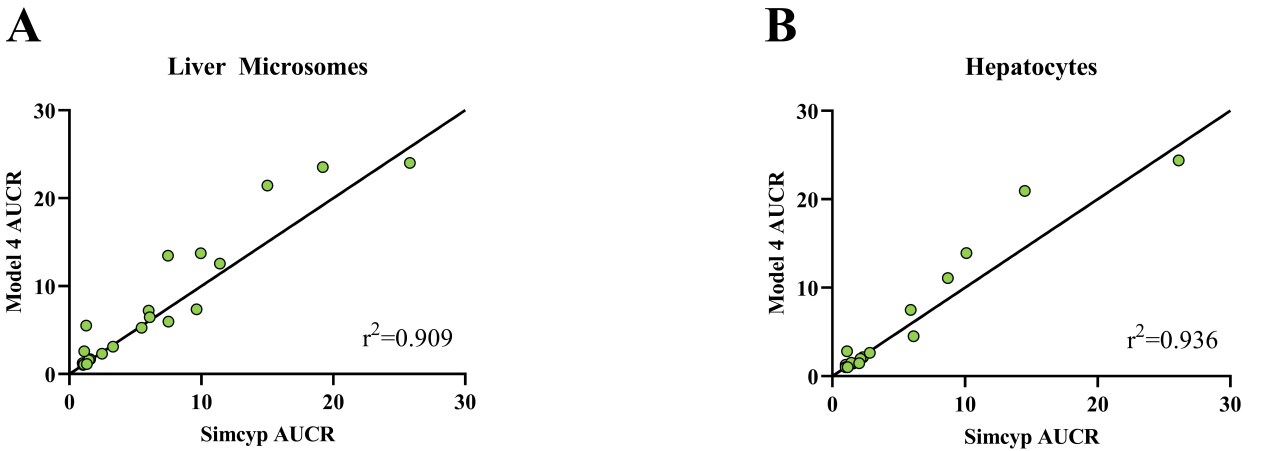
A
Liver Microsomes
Model 4 AUCR
Simcyp AUCR
r2=0.909
0
10
20
30
B
Hepatocytes
Model 4 AUCR
Simcyp AUCR
r2=0.936
0
10
20
30

Figure 6